INTERNATIONAL COMET QUARTERLY

Whole Number 142 | APRIL 2007 | Vol. 29, No. 2

— Table of Contents —

SMITHSONIAN ASTROPHYSICAL OBSERVATORY
60 Garden Street · Cambridge, MA 02138 · U.S.A.

The International Comet Quarterly (*ICQ*) is a journal devoted to news and observation of comets, published by the Smithsonian Astrophysical Observatory in Cambridge, Massachusetts. Regular issues are published 4 times per year (January, April, July, and October), with an annual *Comet Handbook* of ephemerides published normally in the first half of the year as a special fifth issue. An index to each volume normally is published in every other October issue (now in odd-numbered years); the *ICQ* is also indexed in *Astronomy and Astrophysics Abstracts* and in *Science Abstracts Section A*.

The regular (invoiced) subscription rate is US$40.00 per year for North American and for overseas surface-mail delivery (price includes the annual *Comet Handbook*; the price without the *Handbook* is US$30.00 per year). Subscribers who do not wish to be billed may subscribe at the special rate of US$30.00 per year for surface-mail delivery (rate is $20.00 without *Handbook*). Add $20.00/year to each of these rates for overseas airmail delivery. These rates became valid as of Sept. 2005. [The last set of digits (after the hyphen) on the top line of the mailing address label gives the Whole Number that signifies the last *ICQ* issue which will be sent under the current subscription status. An asterisk after these numbers indicates credit for the next annual Comet Handbook. The first five digits represent the subscriber's account number.] Make checks or money orders payable in U.S. funds (and drawn on a U.S. bank) to *International Comet Quarterly* and send to Mail Stop 18; Smithsonian Astrophysical Observatory; 60 Garden St.; Cambridge, MA 02138, U.S.A.

Credit cards may be used for payment of subscriptions, though a minimum of US$20.00 can be accepted for each charge. Credit-card orders may be placed by e-mail (to iausubs@cfa.harvard.edu), by fax (to USA 617-495-7231), or by telephone (to USA 617-495-7280, generally between 14:00 and 21:00 UT, Monday to Friday). When sending orders by fax or e-mail, please include the following information: (1) your name (as given on the credit card); (2) card type (MasterCard, Visa, or Discover); (3) credit-card number and expiration date; (4) address at which the card is registered; (5) which services you wish to subscribe to; (6) if the payment is for the renewal of a current or expired account, please include your account number.

Group subscription rates available upon request. Back issues are $10.00 each — *except* for "current" *Comet Handbooks*, which are available for $15.00 ($10.00 to subscribers if ordered with their *ICQ* subscription; see above). Up-to-date information concerning comet discoveries, orbital elements, and ephemerides can be obtained by subscribing to the *IAU Circulars* and/or the *Minor Planet Circulars* (via postal mail and also available via computer access); for further information, contact the above e-mail address (or the *ICQ* at the above postal address).

Manuscripts will be reviewed/refereed for possible publication; authors should first obtain a copy of "Information and Guidelines for Authors" from the *ICQ* website or from the Editor. Cometary observations should be sent to the Editor in Cambridge; again, see the *ICQ* website or contact the Editor for the proper format. Those who can send observational data (or manuscripts) in machine-readable form are encouraged to do so [especially through e-mail via the Internet (ICQ@CFA.HARVARD.EDU)]. The *ICQ* has extensive information for comet observers on the World Wide Web, including the Keys to Abbreviations used in data tabulation (see URL http://www.cfa.harvard.edu/icq/icq.html). In early 1997, the *ICQ* published a 225-page *Guide to Observing Comets*; this edition is now out of print, but a revised edition is under preparation.

Most of the Observation Coordinators (OCs) listed below have e-mail contacts with the *ICQ* Editor; observers in the general area of such OCs who lack access to e-mail networks may send data to the OC for relay to the *ICQ* in electronic form.

++++++++++++

This issue is No. 142 of the publication originally called *The Comet* (founded March 1973) and is Vol. 29, No. 2, of the *ICQ*. *[ISSN 0736-6922]*

****

IWCA IV

The fourth International Workshop on Cometary Astronomy, co-sponsored by the *ICQ*, is still planned to be held in 2009 in Japan. Akimasa Nakamura reports that the probable dates will be July 25 and 26 (after the total solar eclipse) and that the site will likely be in the Kansai area (Osaka/Kobe), and the IWCA IV will be held jointly with the 39th Japanese Comet Conference. At this point, it is desirable to get an idea of how many participants from outside of Japan are considering attending. Please contact the ICQ Editor to indicate your liklihood of attending the IWCA IV, and this information will be conveyed to the Japanese Local Organizing Committee. Additional information will be posted here and at the *ICQ* webpage on IWCAs.

Forward-Scattering Enhancement of Comet Brightness. I. Background and Model*

*Joseph N. Marcus**
St. Louis, MO, U.S.A.

Abstract. At small scattering angles, θ (= 180° – phase angle), micron-size particles forward-scatter sunlight hundreds to thousands of times more strongly than at side angles, enabling comets to become visible in daylight and even cast shadows at night. In this paper, we comprehensively review forward scattering as it relates to comet dust. We introduce a "compound Henyey-Greenstein (HG)" function, modified by the coma's dust-to-gas light ratio, to model scattering in cometary light curves — the first time this function has ever been applied to comets. To date, only five comets have actually been measured photometrically in forward-scattering geometry. Three of them — C/1927 X1 (Skjellerup-Maristany), C/1975 V1 (West), and C/1980 Y1 (Bradfield) — were assayed by the "gold standard" method of visible-thermal photometry to obtain the coma's energy balance and the scattering (or "phase") function. That of C/1927 X1, reduced from Lampland's unpublished daylight radiometry in Lowell Observatory archives, is presented here in provisional form for the first time. Scattering curves for the other two comets — 96P/Machholz and C/2004 F4 (Bradfield) — are derived from non-thermal SOHO-satellite C3-coronograph photometry (Grynko 2005). Compared to brightness at $\theta = 90°$, the composite light curve shows enhancements of approximately 10-fold at $\theta = 30°$ and approximately 100-fold by $\theta = 13°.5$, the smallest angle at which a comet scattering function has yet been derived. The compound-HG scattering model developed here successfully fits the composite scattering function of these five comets for $\theta \leq 150°$. We show that it also successfully fits scattering data for comets in back-scattering geometry ($150° \leq \theta \leq 180°$), justifying its use for all scattering angles. In application, it correctly predicted the 9-fold brightness surge and naked-eye daylight visibility of comet C/2006 P1 (McNaught) in forward-scattering geometry. This model should prove useful for forecasting brightness enhancements of comets that enter forward-scattering geometry in the future, as well as for analyzing forward scattering in historical apparitions — the subject of subsequent papers in this series.

1. Introduction

A fog layer grows bright in the direction of a low-lying sun. Yet from side-viewing directions, it may be nearly invisible (Fig. 1). This remarkable anisotropy in brightness results from the *forward scattering* of the sunlight by tiny water droplets several to tens of microns in size.

◇ ◇ ◇

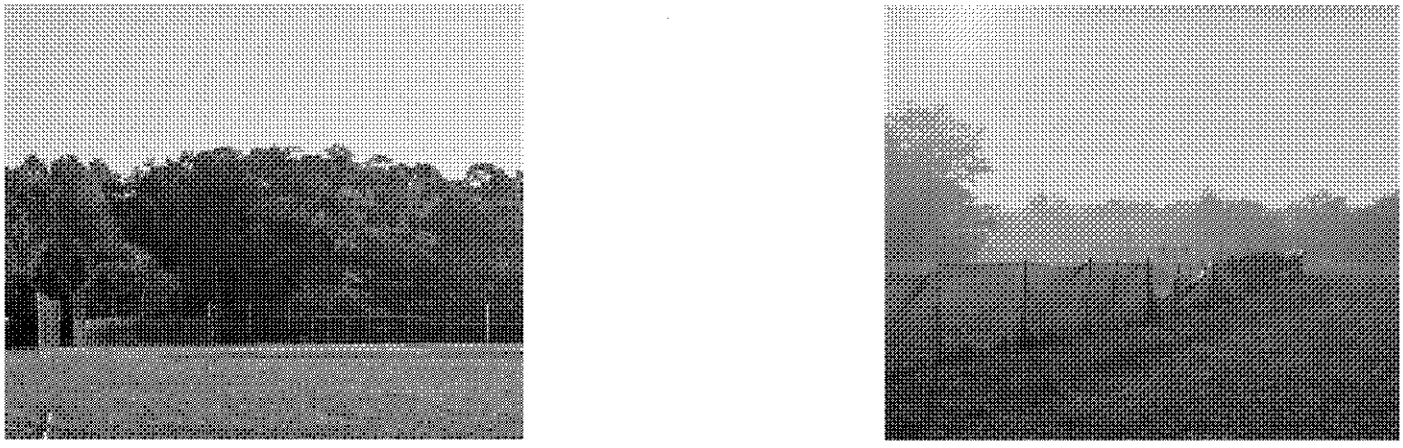

Figure 1. This light fog near sunrise is nearly invisible when viewed from side angles (left panel). Viewed toward the sun, however, it is bright by virture of forward-scattering by its droplets (right panel). Photos by the author.

* Written as a detailed version of a talk presented at the IWCA III, Meudon, France, 2004 June 4–6. Editor's note: previous contributed papers from IWCA III were published over several *ICQ* issues in 2005.

* e-mail address jnmarcus@sbcglobal.net

Cometary comae likewise contain small particles that throw sunlight preferentially in a forward direction. When they come between the earth and the sun — see Figure 2 — comets can flare by factors of tens, hundreds, and possibly thousands over baseline brightness, catapulting them into daylight visibility, and enabling one (C/1861 J1) to even cast shadows at night (Schmidt 1863; Marcus 1997).

◇ ◇ ◇

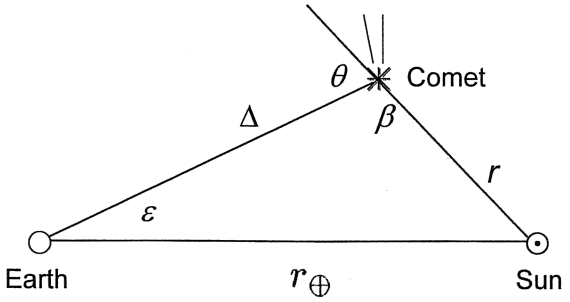

Figure 2. Comet-earth-sun geometry showing the scattering angle, θ; phase angle β; solar elongation, ϵ; and the inter-object distances $r_\oplus$, r, and Δ. θ is the deviation of sunlight from its direction of propagation after scattering, being the supplement of the phase angle (θ = 180° − β).

◇ ◇ ◇

These claims are extraordinary. They demand an examination of the physics responsible for this effect, to ensure the credulity of this remarkable natural phenomenon. This paper will lay that groundwork. We shall review the nature of cometary dust and how it is expected to scatter light. A central purpose of this paper is to introduce a Henyey-Greenstein (HG) function to model the scattering behavior of comet dust — the first time this function has been applied to comets. We shall show that the model successfully fits the composite scattering curve for the five comets that have been measured in forward-scattering geometry to date. These comets collectively show an approximately 100-fold brightness enhancement as the scattering angle, θ (= 180° − phase angle), ranges down to 13°.5, the smallest value at which a comet has yet been measured photometrically. The HG model presented here will prove useful not only in forecasting the brightness surges of comets that enter forward-scattering geometry in the future, but also in analyzing those that have done so in the past — the subject of subsequent papers planned in this series.

Forward scattering is not widely recognized in the comet-science community, no doubt because the geometry is fairly rare, and comets are hard to observe at the small solar elongations at which it occurs. But its effect on cometary brightness is profound and ignored by analysts at their peril. This paper comprehensively reviews the phenomenon in comets for the first time.

2. Background

2.1. Forward Scattering on Earth and in Space

Forward scattering is ubiquitous in the natural world, observed wherever there are suspended small particles and a discrete light source. The earth's atmosphere yields the most familiar examples. The fog of Figure 1 can be quantitatively modeled by the droplets in a cloud chamber, used to detect subatomic-particle paths. Figure 3 shows the brightness of these droplets as a function of the scattering angle (Wilson 1951). This figure, as other figures in this paper, displays the brightness as a scattering function on a logarithmic scale in which the brightness is normalized to 1 (logarithm = 0) at θ = 90°. So extreme are the amplifications that they cannot meaningfully be graphed on linear scales. Notice that for both water and water-alcohol droplets, the brightnesses increase by about 2 log units, or about 100-fold, as the scattering angles decrease from about 90° to 20°. Further severe increases would be expected as θ proceeds from 20° toward 0°, outside of the range of data available for this figure. As θ nears 0°, the final enhancement over θ = 90° for these approximately 10-μm-size particles would be expected to be *thousands*-fold (see Sec. 2.3.5). This explains why the rim of a cloud viewed in the sky to be (apparently) nearly touching the sun's limb (θ ≈ 1°) grows so blindingly bright as to seemingly rival the surface brightness of the sun's disk itself. Such strong forward-throwing behavior is generally diagnostic of particles larger than the wavelength of light — larger than those that typically dominate optically in comet dust (see Sec. 2.2.3).

The cloudless sky itself forward-scatters sunlight due to small atmospheric aerosols and dust particles. This manifests as brightening of the sky toward the sun and is obvious to even the most casual observer. The degree of brightening depends principally upon aerosol concentrations and sizes. Figure 3 shows one example of the scattering function of a clear sky that is relatively free from stratospheric volcanic haze (Volz 1983). Notice that the function is much less steep than for the cloud-chamber droplets: the increase in intensity from θ = 80° to θ = 4°.5 is only 1.18 log units, or 15-fold. There are two reasons for this. First, atmospheric aerosols are smaller than fog droplets, with sizes on the order of 1 μm or smaller (Middleton 1951). As we shall see in Section 2.3.5, smaller particles are less forward-throwing — that is, their forward-scattering peaks are less broad and intense. Second, the aerosol scattering curve is blunted by the intense and relatively flat Rayleigh-type background scattering from small-scale inhomogeneities in the density of air molecules

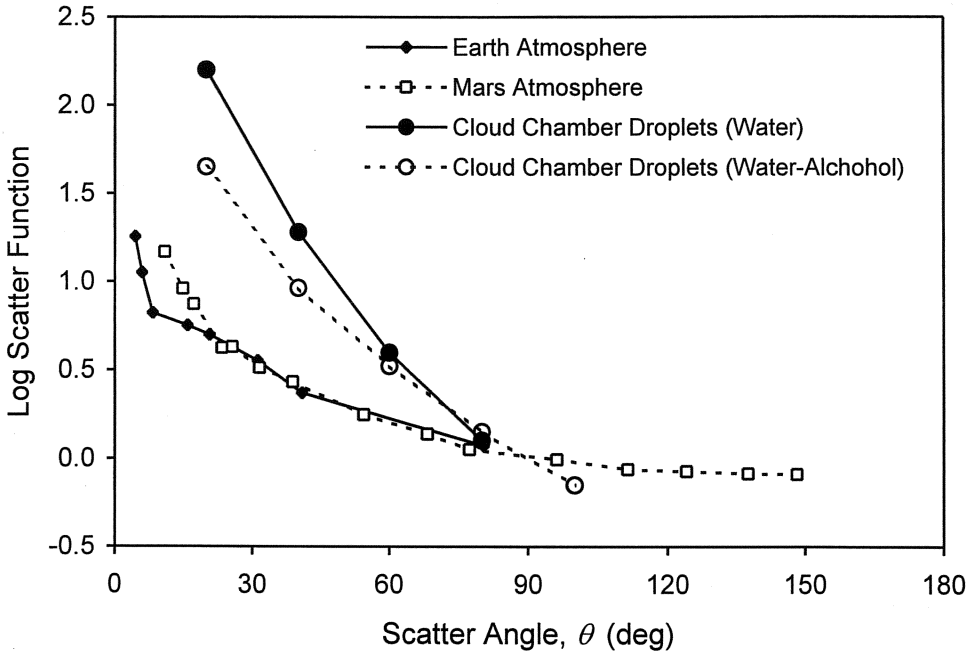

Figure 3. Light-scattering intensity versus scattering angle for water and water-alcohol cloud-chamber droplets (Wilson 1951) and the atmospheres of Earth (Volz 1983) and Mars (Lemmon et al. 2004). The data from these references are normalized here to $\theta = 90°$.

◇ ◇ ◇

[text continued from page 40]

(Sec. 2.3.2). As we shall see in Section 3, the situation is analagous to comet-dust scattering, which competes against background fluorescence emission from gases in the coma.

Also shown in Figure 3 is a scattering curve for the Martian sky as observed from the "Opportunity Mars Exploration Rover" (Lemmon *et al.* 2004). It, too, shows forward scattering. In this case, the scattering particles are fine dust, lofted by winds.

◇ ◇ ◇

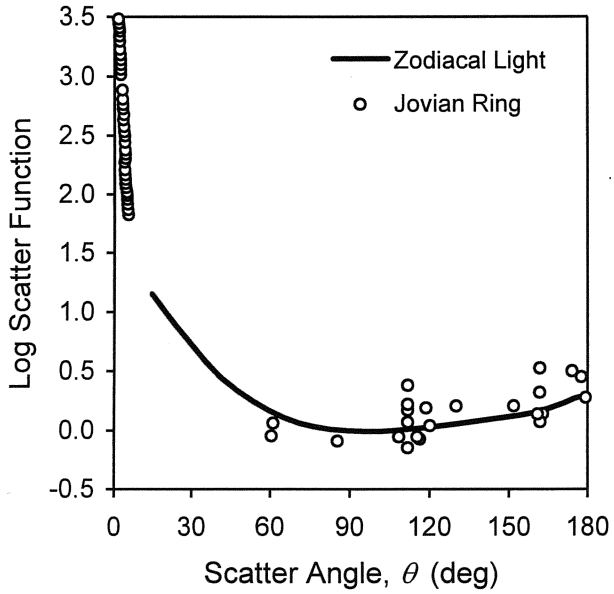

Figure 4. Light-scattering intensity versus scattering angle for the zodiacal-dust band, as modeled by Hong (1985; solid line), and for the dust in the Jovian ring (Porco et al. 2003; circles). The data from these references are normalized here to $\theta = 90°$.

Figure 4 shows scattering by two types of dust in interplanetary space. One is the curve for the zodiacal dust band down to $\theta = 15°$, as modeled by Hong (1985). The other is the scattering function for the dust ring of Jupiter as measured by instruments aboard the *Voyager*, *Galileo*, and *Cassini* spacecraft (Porco *et al.* 2003). Jupiter's ring shows an amazing 3.5-log (3000-fold) increase in scattering brightness as the scattering angle declines from side viewing to $\theta = 1°.6$ (Fig. 4). If extrapolated to $\theta \approx 0°$, the total enhancement could well reach 10000 or more. The spacecraft measurements show that, in the interval of $\theta = 6°.0$ to $1°.6$ alone, the ring brightness increases a hundred-fold (Fig. 11.8 in Burns *et al.* 2004)! Such radical behavior diagnoses the presence of large particles of size ≈ 15 μm (Porco *et al.* 2003), larger than those thought to optically dominate comet dust (see Sec. 2.2.3). Larger particles are more narrowly and intensely forward scattering. But as we shall see in Sections 4.3 and 5, forward scattering by the larger-particle component of comet dust may be detectable in some circumstances.

◇ ◇ ◇

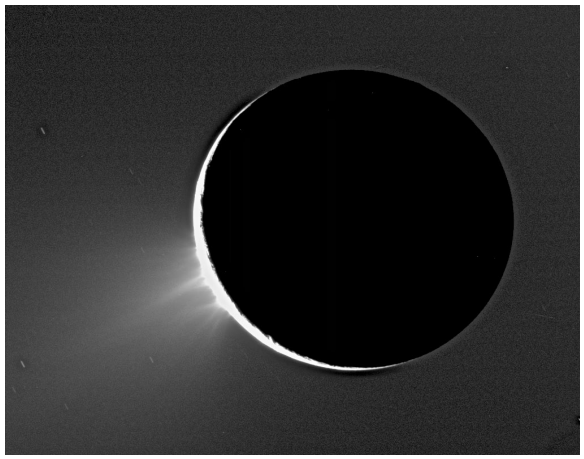

Figure 5. The first direct imaging of the ice-volcano plumes on Enceladus, backlit by the sun at a scattering angle of $\theta \approx 21°$. Forward-scattering of the sunlight greatly enhances their visibility. The fountains feed micron-size particles into Saturn's optically thin 'E' ring, visible here as a faint forward-scatter amplified glow that silhouettes the dark side of the satellite. Image courtesy of NASA/JPL/Space Science Institute.

◇ ◇ ◇

Figure 5 is the first direct visible image of the eruptions of water volcanoes on the satellite Saturn II (Enceladus), acquired in 2005 November by the Cassini mission. These volcanoes had long been suspected as sources of Saturn's broad and tenuous 'E' ring, which is composed of particles on the order of 1 μm in size (Pang *et al.* 1984; Kempf *et al.* 2005). Based on the ratio of the width of the illuminated crescent to the satellite's diameter, I compute the scattering angle as $\theta = 21°$ in this view. Strong forward-scattering geometry must greatly enhance the brightness of the E ring, whose glow silhouettes the dark side of the satellite in this picture. For 1-μm-size particles, forward-scattering brightness enhancements in the range of 10- to 50-fold would be expected. Thus, forward scattering aided in the detection of the volcanic plumes on Enceladus.

2.2. The Nature of Cometary Grains

2.2.1. History

Evidence that comets contain dust is longstanding [see the good reviews in Yeomans (1991), Sekanina *et al.* (2001), Festou *et al.* (2004a), and Fulle (2004)]. The polarization of light, indicative of microscopic particles, was observed by D. F. J. Arago in the tail of C/1819 N1 (Thralles), and spectroscopy of comets beginning in the 19th century showed a solar-continuum component thought to be due to reflecting solid material in the coma and tail. Hevelius drew structures in the coma of Halley's comet in 1682 that we today recognize as dust. Their dynamical behavior during the same comet's 1835 apparition led Friedrich W. Bessel in 1836 to introduce the concept of a repulsive force from the sun acting on particles, which Euler identified as radiation pressure. At the end of the 19th century, Fyodor A. Bredikhin invoked this concept in his studies of tail formation, as did Finson and Probstein (1968) in modern times. Schiaparelli's linkage of the orbits of the Perseid and Leonid meteors to those of comets 109P/Swift-Tuttle and 55P/Tempel-Tuttle, respectively, reinforced the association between comets and meteoric dust. The reconnaissance spacecraft to 1P/Halley in 1986 directly demonstrated the existence of dust in this comet in a wide range of sizes from 10^{-22} g to $> 10^{-5}$ g (*e.g.*, McDonnell *et al.* 1987).

2.2.2. Properties Deduced from Observations

Kolokolova *et al.* (2004a) have summarized what we know about the physical properties of comet grains from observations. The grains have low geometric albedo, indicating that they absorb light. They manifest strong forward scattering, weak back scattering, and a flat brightness profile in between. They polarize light, with weak negative polarization (-2

percent) for $\theta > 160°$ and strong positive polarization (10-30 percent) for $\theta < 159°$, with a broad maximum at $\theta = 80°$-$90°$ (*e.g.*, Levasseur-Regourd *et al.* 1996). The degree of polarization with respect to the wavelength, λ, of light — the "polarimetric color" — generally increases for $\theta < 150°$. The presence of slight circular polarization (< 2 percent) indicates that the particles are non-spherical and/or optically active. Comet dust is usually red to varying degrees over a broad range of λ, which is attributable to particles that are at least slightly absorbing and larger than subwavelength to wavelength sizes.

Comet dust re-emits the light energy that it absorbs as heat in the infrared. The infrared spectra often show temperatures, T, in excess of what would be expected for a black body at the given distance from the sun, characterized as a "superheat" ($S = T_{\rm comet}/T_{\rm BB} > 1$), as well as a silicate emission band located at ≈ 10 μm. These two features are diagnostic of constituent submicron absorbing grains. The fact that thermal emission at $\lambda > 20$ μm does not decrease more steeply than that of a theoretical black body indicates that the dust lies in a broad size distribution that includes particles > 1 μm in size.

The brightness, polarization, color, and infrared emission properties of comet grains are together consistent with either (1) irregular, different-size ("polydisperse"), but predominantly submicron particles, or (2) porous aggregates, some of them large, of submicron particles (Kolokolova *et al.* 2004a).

2.2.3. Dust Size Distribution and the Concept of "Optically Important Grains"

The comet dust-size distribution is most often modelled in the form

$$n(R) \propto R^{-p}, \tag{1}$$

where $n(R)$ is the number of particles, R is the particle radius,[1] and p is the power-law index. As an example of how this distribution works, if $p = 3$, a particle twice as large as another is $2^{-3} = 1/8$ as abundant. The smaller the value of p, the more shallow the size distribution and the greater the relative concentration of large particles, while larger p gives steeper distributions with dust mass more concentrated in smaller particles. The tipping point is $p = 3.5$ (Fulle 2004). Based on dust-tail morphologies, Fulle (2004) finds $3 \leq p \leq 4$ for nearly all comets that he has analyzed. But tail particles are not perfectly representative of native grains, for they have been sorted by radiation pressure and have partly evaporated. *In-situ* data from the *Giotto* spacecraft reconnaissance of 1P/Halley show that $p < 3$ — *i.e.*, mass is concentrated in large particles (McDonnell *et al.* 1987).

The Finson and Probstein (1968) theory of dust-tail dynamics indicates that the optically dominant particle size in the coma and tail is about a micrometer, a conclusion supported later by infrared observations of excess grain temperatures and silicate spectral signatures present in many comets (Ney 1982). Gehrz and Ney (1992) refer to these as "optically important grains", and mean effective sizes $R_{\rm eff} \approx 0.5$ μm are generally accepted in the literature (Jewitt 1991; Kolokolova *et al.* 2004). This is not to say that a significant — indeed, a majority — mass fraction of dust may not exist in larger grains, but they are optically unimportant. As an example, the "gassy" comet 2P/Encke is notoriously deficient in optically observable dust — yet, from infrared observations, it has a considerable "dust" mass locked up in larger, optically unapparent particles of $R_{\rm eff} \geq 20$ μm (Lisse *et al.* 2004).

The inference of the optical dominance of micron-size grains is important when we come to consider how comets scatter sunlight. As we shall see in Section 2.3.5, the degree of forward scattering depends powerfully upon particle size.

2.2.4. Comet Heterogeneity

Although similar to one another, comets also manifest differences. For example, there is a 1.4-dex (25-fold) difference in the dust-to-gas ratio in the large sample studied by A'Hearn *et al.* (1995). The *Stardust* and *Deep Impact* comet missions show that comets 81P/Wild and 9P/Tempel are heterogeneous mixtures of primordial interstellar grains, on the one hand (Sec. 2.2.5), and altered minerals, including some processed in hot central regions of the early solar nebula, on the other (A'Hearn 2006). Perhaps differing proportions of these ingredients from comet to comet could account for observed differences in cometary characteristics that we explore below.

In recent years, infrared photometry has defined two classes of comets: "IR Type I", with minimal superheat ($S \simeq 1$) and weak or absent 10-μm silicate emission; and "IR Type II", with substantial superheat ($S \gtrsim 1.2$) and usually strong silicate emission (Gehrz *et al.* 1989; Gehrz and Ney 1992; Gehrz 1997). "Gassy" comets are generally of "IR Type I" — having weak optical continua and lacking prominent dust tails — while those of "IR Type II" have stronger continua and often spectacular dust tails. "Type I" comets tend to be short-period objects that are thought to originate from the transneptunian cubewano belt, while "Type II" comets tend to be long-period bodies from the Oort Cloud (Soderblom *et al.* 2002). The "Type II" infrared features, commonly attributed to the presence of smaller, hotter, submicron grains (*e.g.*, Mason *et al.* 2001), may be better explained by higher porosities of aggregated grains (Li and Greenberg 1998; Kolokolova and Kimura 2006).

The type-I and -II classification scheme cannot be absolute, for there is the example of C/1996 B2 (Hyakutake), which manifested both types-I and -II behavior over the course of its apparition, indicating different kinds of dust sources on its nucleus (Mason *et al.* 1998). There is also comet C/1995 O1 (Hale-Bopp), an example of a "Type II" comet of such extreme degree (Mason *et al.* 2001) as to arguably place it in a class by itself.

---

[1] Note that the variable a is often used by authors in the literature on dust scattering. The *ICQ* Editor prefers upper-case R to be used always for radius or distance from a cometary nucleus, because a is standard usage in cometary astronomy for semi-major axis and lower-case r is standard usage in cometary astronomy for heliocentric distance. Deviations from these standard usages in the literature is not helpful to readers. – Ed.

It has been proposed that comets also have two polarization classes — low and high — which respectively correlate to infrared types I and II (Levasseur-Regourd *et al.* 1996). However, Jockers *et al.* (2005) suggest that the division into polarization classes is an artifact of contamination of the spectrum by light from the gasses.

To the extent that the infrared type-I and -II classification reflects real differences in comets — which on balance it seems to do — we should expect an impact on the forward-scattering brightness behavior of comets. For "Type I" comets, the comparatively stronger spectral-line emissions relative to the dust continuum — particularly from C_2 in the visible — should blunt forward-scattering brightness enhancement more than for "Type II" comets. We take into account this blunting effect when we come to model the comet scattering function in Section 3.

2.2.5. The Greenberg Interstellar Dust Comet Model

Greenberg (1982, 1998, 2000; Greenberg and Li 1997) proposed a model of cometary nuclei as loose, porous aggregates of elongated, interstellar-dust grains of size $\approx$ 0.2 to 0.4 μm. These contain elongated, $\approx$ 0.1- to 0.2-μm, rocky, silicaceous cores — which are surrounded by a mantle of refractory organic sludge and frosted by an outer coat of volatile ices. Mixed into the ices are ultrafine, carbonaceous particles of size $\approx$ 0.002 μm and polyaromatic hydrocarbon macromolecules of size $\approx$ 0.005 μm (see Fig. 6). This overall composition and structure is deduced from the observed ultraviolet, visible, and infrared absorptions, emissions, and polarizations of the dust in interstellar space (Greenberg 2000).

◇ ◇ ◇

Figure 6. Scaled-up acrylic "bird's nest" model built by J. Mayo Greenberg (1922-2001) to simulate comet dust as aggregates of constituent interstellar grains. The processed grains have elongated, 0.1- to 0.2-μm silicate cores (salmon-colored), which are coated by refractory organic and icy mantles (clear- to blue-colored). The mantles are peppered with innumerable nanometer-size carbon-rich particles and polyaromatic hydrocarbon macromolecules (the tiny black flecks). Models like these, matched for inferred refractive and absorptive properties, are used to study the scattering properties of comet dust using microwaves instead of visible light. Image courtesy of Naomi Greenberg.

◇ ◇ ◇

The silicaceous cores originate in the atmospheres of red-giant stars, which spew them into interstellar space, where they find their way into ultra-cold gas clouds. There the gases condense onto them as ices, which anneal into refractory organic tars under the relentless punishment of ultraviolet radiation. The grains cycle in and out of variably dense interstellar dust and molecular clouds over hundreds of millions to billions of years, building up their refractory mantles. In the protoplanetary solar nebula, these highly processed grains gained a final ice frosting as they condensed into cometary nuclei some 4.6 billion years ago. The result is a fluffy, highly porous composite of grains resembling the "bird's nest" model in Figure 6. When heated by the sun, comets release various-sized aggregates of these grains, which we observe as the "dust". Such particles, recovered from the earth's stratosphere (Brownlee 1978), resemble Greenberg "bird's nest" aggregates.

The Greenberg model has been immensely influential in contemporary cometary science (Marcus 2001), having been endorsed by no less than Fred L. Whipple (1987), the originator of the "dirty snowball" model of the comet nucleus (Whipple 1951). The Greenberg model drives many of the simulations of comet-dust light scattering that are considered

in the next section. At the same time, we know that comets are not pure Greenberg-type dust, because they also contain rocky minerals processed in the hotter central regions of the primordial solar nebula (*e.g.*, A'Hearn 2006).

2.3. The Scattering Behavior of Small Particles

2.3.1. Computational and Experimental Models

The scattering function of comet grains at small scattering angles, especially very small θ, is not that well known. To explore these regions, it is helpful to *simulate* the behavior with either computational or experimental models.

Maxwell's electromagnetic theory of light, brought forth in 1864, is the basis for computing how light scatters off particles. In practice, precise solutions of Maxwell's equations are tractable only for spheres, spheroids, and cylinders. Mie (1908) consolidated the scattering equations for homogeneous spherical particles, and in the mid-20th century, Van de Hulst (1981) — and more recently Bohren and Huffman (1983) — provided computational techniques to apply "Mie theory" for larger ranges of particle sizes and refractive indices. For very small particles of subwavelength sizes, Rayleigh theory can also be employed. Our considerations here involve *single scattering* — that is, one scattering event — which applies to particle clouds of low optical depths ($\tau < 0.1$; Van de Hulst 1981) that are typical of comets.

In the treatment of scattering, two parameters are of interest. One is the complex refractive index

$$m = \nu - \kappa i, \tag{2}$$

a complex number, where ν is the real component that is responsible for refraction, and κ is the coefficient of the so-called "imaginary" component, i ($i^2 = -1$), that is responsible for absorption. The other is the dimensionless, universal size parameter

$$X = \frac{2\pi R}{\lambda}, \tag{3}$$

where R (cf. equation 1) is the particle radius and λ is the wavelength of light. For a given X, the scattering behavior of electromagnetic waves is identical across widely different parts of the spectrum, so long as the wavelength-dependent ν and κ values of the materials can be replicated. This "principle of electromagnetic similitude" (Gustafson 1996) can be exploited by the use of scaled-up centimeter-size models (Fig. 6) and microwaves to simulate the scattering of visible light by micron-size particles — the "microwave analog" technique pioneered by Greenberg *et al.* (1961). This method has been profitably employed in microwave laboratories to model cometary and interplanetary dust scattering (Giese 1980; Greenberg 1980; Greenberg and Gustafson 1981; Zerull *et al.* 1993; Gustafson 1996; Gustafson and Kolokolova 1999). Comet dust can also be experimentally modeled directly with visible light using suspensions of small particles in air streams and in microgravity environments (reviewed in Kolokolova *et al.* 2004a).

In reality, the scattering behavior of particles like comet grains differs significantly from that of idealized Mie spheres. Solutions for Mie spheres introduce resonances in the scattered intensity and polarization that are not as conspicuous in nonspherical particles and that are not observed in comets (Yanamandra-Fisher and Hanner 1999). The factors that contribute to the departure from "Mie behavior" are particle shape (non-sphericity) and compositional heterogeneity. But the numerical modeling of scattering by non-Mie particles, either as constituent units ("monomers") or monomer aggregates, is complicated, straining the capacities of even the most advanced computer platforms. The computation times required increase exponentially with the number of constituent particles in aggregates, placing practical limitations on the size of aggregate that can be modeled.

Two computing methods for modeling non-spherical particles are currently popular (Kolokolova *et al.* 2004b). In the "discrete dipole" approximation (DDA), the comet grain is represented as an ensemble of polarizable units, or dipoles; it relies upon solutions for the internal electromagnetic field (inside the grain), from which the scattered field (outside the grain) is calculated. The other, the "T-matrix" approach, is based on the solution of field differential equations for the particle that satisfy the boundary conditions at its surface; it works well and is fast for randomly oriented particles.

The comet-dust scatter-modeling literature is very active and exponentially expanding. Good review sections can be found in recent papers by Jockers (1997), Petrova *et al.* (2000), Hadamcik *et al.* (2002), Kimura *et al.* (2002, 2003), and Kolokolova *et al.* (2004a, 2004b). One senses optimism that the models are inching closer to replicating all optical and thermal properties of cometary dust — the scattering function, polarization, color, polarimetric color, the superheat, and the infrared silicate emission spectrum. These improvements in turn will help to better define the nature of comet dust and thereby constrain its scattering function. In the next sections, we give just a few examples of what Mie and non-Mie models tell us about light scattering by comet dust.

2.3.2. Rayleigh and Mie Scattering Regimes

Figure 7 shows scattering intensities for different-sized absorbing Mie spheres, computed using 'ScatLab' freeware (`http://www.scatlab.com`). I chose the refractive indices $\nu = 1.9$ and $\kappa = 0.50$, which are thought to reasonably represent cometary material (Kimura *et al.* 2006). The panels display the scattered light's perpendicular and parallel, polarized electric-field components and their summed intensities. The figure demonstrates a number of important points:

1) The scattering curve of the $X = 0.5$ sphere is fairly flat — there is only minimal forward scattering (≈ 0.3 log units, or two-fold). This is a characteristic of Rayleigh-regime scattering by particles that are significantly smaller than the wavelength of light, irrespective of their shapes. In the deep-red light of this example ($\lambda = 0.63$ μm), the sphere radius is $R = 0.05$ μm (see equation 3).

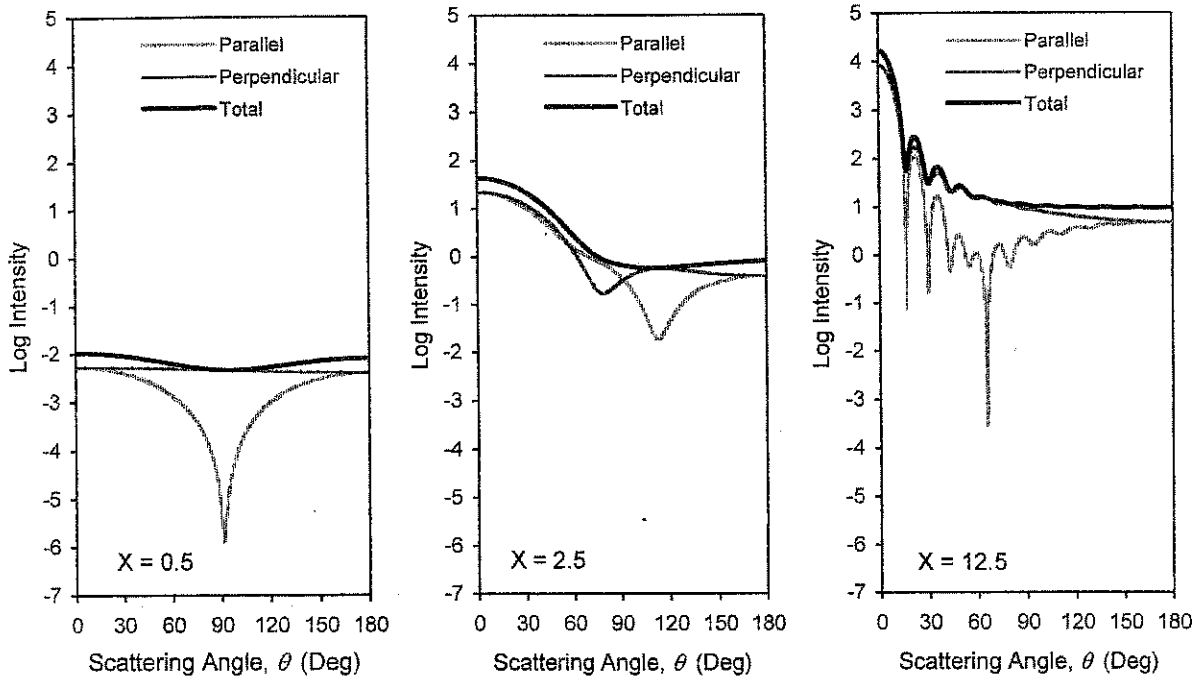

Figure 7. Light-scattering intensity vs. scattering angle, computed for different-sized absorbing Mie spheres in deep red light ($\lambda = 0.63$ μm). At this wavelength, the sizes (X) correspond to radii of $R = 0.05$ μm (left), 0.25 μm (center), and 1.25 μm (right), respectively (see equation 3). The refractive index is taken as $m = 1.90 - 0.50i$ (see equation 2), similar to that inferred for comet grains. Each panel shows the polarized components parallel and perpendicular to the scattering plane and their summed intensities. The smallest sphere manifests a flat scattering curve typical of Rayleigh-regime scattering, while the larger ones display a strongly forward-throwing peak that heightens and narrows with increasing particle size.

◇ ◇ ◇

[text continued from page 145]

2) In contrast, the $X = 2.5$ ($R = 0.25$ μm) sphere — comparable in size to the wavelength of light — shows strong forward scattering, about 1.7 log (50 times) stronger than side-angle scattering.

3) As the size increases (to $X = 12.5$, or $R = 1.25$ μm in the figure example), the intensity of the forward scattering increases (to 3.2 log, or 1600 times), and the peak narrows.

4) There are peaks and troughs in the scattering functions of the $X = 0.5$ and $X = 2.5$ spheres, resulting from internal interferences by the wavefronts. For actual comet dust, these intensity irregularities would be smoothed out by a particle-size distribution such as in equation 1, as well as by irregularities and variations in shapes and orientations of particles and by ranges in the wavelengths of the light source.

5) The scattered light is *polarized* — that is, its components that are perpendicular and parallel to the scattering plane are unequal. Comet-dust light scattering likewise is polarized (see Sections 2.2.2 and 2.2.4).

For wavelength-size and larger particles, the scattering intensity is proportional to the cross section — *i.e.*, $\propto R^2 \propto X^2$ (van de Hulst 1981). But for smaller particles in the Rayleigh scattering regime, the scattering efficiency scales as X^{-4} (van de Hulst 1981), or equivalently, as R^4 or as λ^{-4} from equation 3. That is why the daylight sky — dominated by Rayleigh scattering by small-scale inhomogeneities in air density — appears blue to the eye. By the same token, because cometary dust is not blue (Sec. 2.2.2), smaller particles do not dominate optically in light scattering by comet dust. Subwavelength-size particles simply do not scatter light efficiently. We can see this effect in Figure 7. The average scattering intensity of the $X = 0.5$ sphere is about 2 log (100 times) less than that of the $X = 2.5$ sphere — yet its relative cross section is $(0.5/2.5)^2$, or 25 times less.

From the foregoing considerations — the optical *unimportance* of scattering by model particles and actual comet dust of subwavelength sizes, and the optical *importance* and *forward-throwing* nature of scattering by particles of wavelength and larger sizes — we can securely conclude that *comet-dust scattering must be strongly forward-throwing.* This principle is important. By implication, any comet in which dust contributes significantly to its light — *i.e.*, most comets — should display significant forward-scattering brightness enhancement. This prediction is supported in Sections 4.2 and 4.3.

2.3.3. The Smoothing Effect of a Size Distribution

A particle-size distribution such as the one in Equation 1 smoothes the resonant "bumps" present in the scattering function of single particles like the one depicted in Figure 7b (Giese 1963; Ney and Merrill 1976; Greenberg and Gustafson

1981; Petrova *et al.* 2000). Figure 8 shows a "T-matrix" computation of the scattering curve for a collection of different-size particle clusters (Petrova *et al.* 2000). The aggregates consist of between 8 and 43 'unit' ("u") monomers of $X_u = 1.3$ size ($R_u = 0.13$ μm at $\lambda = 0.63$ μm, from Equation 3), simulating the Greenberg constituent interstellar-grain size, in a size distribution of index $p = 3.0$ (cf. Equation 1), giving the aggregrates an effective radius of $R_{\rm eff} = 0.35$ μm. In the simulation, $\nu = 1.65$, near the refractive index of silicates, and the monomers are slightly absorbing ($\kappa = 0.01$). We see that the scattering curve of this distribution of different-sized particles is very smooth.

◇ ◇ ◇

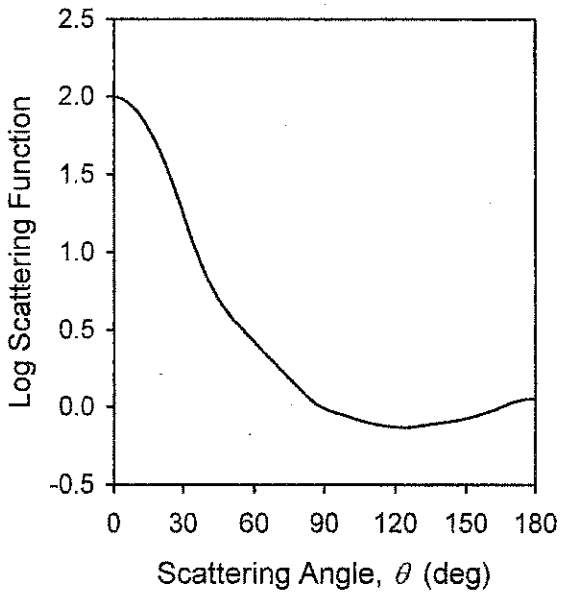

Figure 8. A distribution in particle sizes smoothes out the "peaks" and "valleys" in the scattering curves of small particles caused by interference effects (cf. Fig. 7). Data from Petrova et al. (2000) are normalized here to $\theta = 90°$.

◇ ◇ ◇

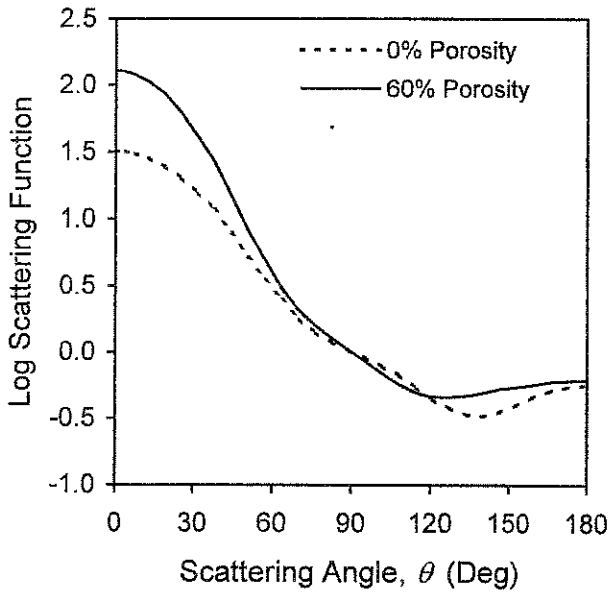

Figure 9. Scattering for porous and non-porous silicate tetrahedra of size $X = 2.5$, computed by the DDA method and averaged over many orientations. Porosity increases forward-scattering. Data adapted from Fig. 13 of Yanamandra-Fisher and Hanner (1999) and normalized here to $\theta = 90°$.

◇ ◇ ◇

2.3.4. The Effect of Grain Structure

In "microwave analog" simulations of Greenberg-type (Greenberg and Hage 1990) dust aggregates, the addition of organic mantles to silicaceous cores increases forward scattering (Zerull *et al.* 1993). Porosity, shape, and composition also affect scattering. Using the DDA computational method, Yanamandra-Fisher and Hanner (1999), for example, find that increasing the porosity gives steeper and stronger forward-scattering (Fig. 9).

2.3.5. The Effect of Particle Size

Forward scattering is largely a result of diffraction. As such, it is increasingly independent of the particle composition, porosity, structure, *etc.*, as the particle size increases. As noted in section 2.3.2, above, its amplitude is proportional to R^2 (and X^2), regardless of particle shape or refractive index (Bohren and Huffman 1983). Compared to side-angle scattering at $\theta = 90°$, the enhancement at $\theta = 0°$ by particle size is considerable, even astonishing, in the examples already provided — from 2 times to 50 times to 1600 times for the $X = 0.5$, 2.5, and 12.5 Mie spheres of Figure 7, or from 130 times for the $X = 2.5$ porous tetrahedra of Figure 9 to 3000 times for Jupiter's 15-μm ($X = 90$ in visible light) ring particles in Figure 4. For even larger particles — *e.g.*, the $X = 600$ (diameter $\approx$ 0.1 mm in visible light) Mie spheres in Figure 13.4 of Bohren and Huffman (1983) — the forward-scattering enhancement is 6.5 log (3000000 times!), but almost all of it (4.5 log worth) occurs within $\theta \leq 5°$. For very large particles ($X \gtrsim 1000$), about half the scattering flux is concentrated within $\theta \leq 170°/X$ (Vaidya and Desai 1986).

These size effects are seen specifically in Greenberg-type aggregate models of comet dust. Kimura *et al.* (2003) used the "T-matrix" method to simulate aggregates of monomer spheres of radii $R = 0.1$ μm (Greenberg and Hage 1990). They studied two types of aggregates: the "ballistic cluster-cluster aggregation" (BCCA), formed by the sticking together of identical monomer clusters moving in ballistic trajectories, and the "ballistic particle-cluster aggregation" (BPCA), formed by the sticking of ballistic monomers onto monomer clusters (Mann *et al.* 2004). BCCAs are highly porous, while BPCAs are relatively compact, and each represent plausible ways by which comet grains accreted in the pre-solar nebula. Using the inferred elemental composition of comets, with carbonaceous materials dominating over silicates, Kimura *et al.* derive $\nu = 1.88$ and $\kappa = 0.47$ for the aggregates in blue light ($\lambda = 0.45$ μm). Figure 10 shows the scattering function for 64-monomer and 256-monomer BCCA aggregates, corresponding to volume-equivalent radii of 0.400 and 0.635 μm, respectively. Although the difference in sizes is slight, the larger aggregate still is more forward-throwing at more-narrow angles. The results were similar for BPCAs. Using the DDA method, Kozasa *et al.* (1993) obtained similar results, although their monomer spheres were smaller than the constituents postulated in the Greenberg model. Relative to $\theta = 90°$, forward scattering of red light ($\lambda = 0.6$ μm) at $\theta = 0°$ for their BCCA aggregates increased from 12-fold to 230-fold as aggregate-characteristic radii increased from 0.205 μm (256 monomers) to 0.993 μm (4096 monomers).

◇ ◇ ◇

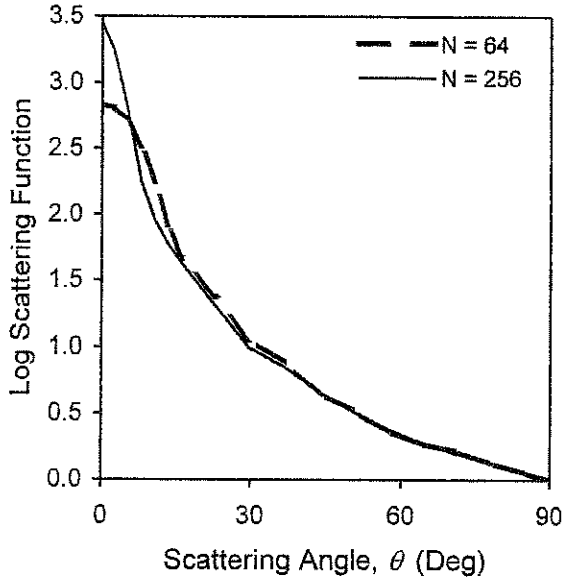

Figure 10. Increasing the particle size narrows and increases forward-scattering. 'T-matrix' simulations in blue light of Greenberg-type BCCA dust aggregates composed of 64 or 256 0.1-μm-radius monomers. The effective radii of the aggregates are 0.400 and 0.635 μm, respectively. Data adapted from Fig. 1 of Kimura et al. (2003) and normalized here to $\theta = 90°$.

◇ ◇ ◇

3. Modeling the Cometary Scattering Function, $\Phi(\theta)$

3.1. Derivation of the Function

The total brightness of a cometary coma

$$I(\theta) = I_G + I_D(\theta) + I_N(\theta) \tag{4}$$

derives mainly from the light of its gas (G) and dust (D); in the inner solar system, the relative contribution from the nucleus (N) is negligible. C_2 comprises most of the gas component in the visual scotopic passband (Newburn 1981, 1984). The fluorescing gasses emit light isotropically — that is, equally in all directions — so I_G is independent of the scattering angle, θ. But we know from Section 2 that the scattered light of $I_D(\theta)$ must exquisitely depend on θ, with strong forward scattering and weak back scattering expected. We express the behavior of $I_D(\theta)$ as the normalized dust-scattering function

$$D(\theta) = \frac{I_D(\theta)}{I_D(90°)}, \tag{5}$$

where $I_D(90°)$ is the dust brightness viewed by convention at $\theta = 90°$ (*e.g.*, Greenberg and Gustafson 1981; Newburn 1981; Hong 1985). How much that the pure dust scattering contributes to total coma brightness depends on the amount of competing gas light in the coma. Its relative strength can be characterized by the dust-to-gas light ratio

$$\delta_{90} = \frac{I_D(90°)}{I_G}, \tag{6}$$

defined at $\theta = 90°$. This quantity is very dependent upon the wavelength passband that we specify, whether it be human visual (discussed in Sec. 3.5) or non-visual (the instrumental photometry analyzed in Sections 4.2-4.4). The most prominent gas emission is from C_2, which lowers δ_{90} in the visual passband. Ignoring the $I_N(\theta)$ term in Equation 4, we can define the total coma scattering (or "phase") function as

$$\Phi(\theta) = \frac{I(\theta)}{I(90°)} = \frac{I_G + I_D(\theta)}{I_G + I_D(90°)}. \tag{7}$$

Substituting for I_G and $I_D(\theta)$ via Equations 5 and 6 transforms Equation 7 into

$$\Phi(\theta) = \frac{\delta_{90}}{1 + \delta_{90}}\left[D(\theta) + \frac{1}{\delta_{90}}\right]. \tag{8}$$

This is the central equation of our model. Note its properties:

1) $\Phi(\theta) < D(\theta)$ for all δ_{90}.
2) $\Phi(\theta) \to D(\theta)$ as $\delta_{90} \to \infty$; *i.e.*, for large δ_{90}, the coma's scattering function is effectively the dust-scattering function. This situation occurs in human visual observations when the relative gas contribution to the coma light is very small, as when a comet is intrinsically very "dusty" or at very small or large heliocentric distances (Sec. 3.5), or in instrument observations when the coma is measured in filters designed to isolate the continuum.
3) $\Phi(\theta) \to [1 + \delta_{90}D(\theta)] \to 1$ as $\delta_{90} \to 0$; *i.e.*, for very small δ_{90}, there is no effective coma-scattering function. This situation obtains in human visual observations when the relative gas contribution to the coma light is very large, as when a comet is intrinsically very "gassy", or in instrument observations when the coma is measured in filters designed to isolate emission bands.
4) $\Phi(\theta) = 1$ when $D(\theta) = 1$; *i.e.*, like $D(\theta)$ in Equation 5, $\Phi(\theta)$ is unity (or "normalized") at $\theta = 90°$.

Pursuing this last point, "normalization" (proportionately adjusting a function to 1, or its logarithm to 0, at a preferred point) is a handy device that we employ throughout this paper in many of the equations and figures. Normalizing $\Phi(\theta)$ at a preferred value of $\theta = 90°$ is a logical choice, for as we shall see in Section 4, this comet-scattering function is relatively flat — *i.e.*, $\Phi(\theta) \approx \Phi(90°) = 1$, and $\log \Phi(\theta) \approx 0°$ over the side-scattering regime of $70° \lesssim \theta \lesssim 160°$. This is the range over which most comet observations are made. In this region, scattering effects can be (and usually are) ignored, and with the $\theta = 90°$ normalization scheme, the scattering terms conveniently drop out of the equations for cometary brightness (Equations 9 and 10, below).

Modeling $\Phi(\theta)$ in Equation 8 is a prime mission of this paper. Therefore, we shall closely examine its components, $D(\theta)$ and δ_{90}, in Sections 3.4 and 3.5, after some brief remarks on cometary brightness and the scattering function in the next two sections.

3.2. Relation to Cometary Brightness

$\Phi(\theta)$ appears in the familiar formulae for a comet's total-coma brightness and magnitude as

$$I_1(\theta) = I_0 \Delta^{-k} r^{-n} \Phi(\theta) \tag{9}$$

and

$$m_1 = -2.5 \log I_1(\theta) = m_0 + 2.5k \log \Delta + 2.5n \log r + m_{\Phi(\theta)}, \tag{10}$$

where I_1 (and m_1) are the total brightness (and magnitude) of the *whole* coma (denoted now by the subscript '1'); r and Δ are respectively the comet-sun and comet-earth distances in astronomical units (AU); I_0 (m_0) is the "absolute"

brightness (magnitude) defined at $r = 1$ AU $= \Delta$; n and k are the indices of brightening, with n found usually to be near 3-4 (Meisel and Morris 1982), and k usually assigned as 2 (inverse-square law, no "delta effect"[2]); and $m_{\Phi(\theta)} = -2.5 \log \Phi(\theta)$ is the magnitude of the scattering function, being negative when $\Phi(\theta) > 1$.

The coma's scattering function is almost invariably ignored in analyses of cometary brightness; *i.e.*, $\Phi(\theta)$ is assumed to be 1. Generally this is safe to do, because comets are almost always observed in the range $70° < \theta < 160°$, where the function is almost flat. There is a well-recognized *back-scattering* enhancement in coma brightness as a comet approaches opposition in the range $150° < \theta < 180°$. This increase is modest but noticeable, in the range of $\Phi(\theta) \approx 1.5$-4 in Equation 9, or up to about 1.5 magnitudes in Equation 10. In contrast, the impact of *forward-scattering* enhancement on $\Phi(\theta)$ and comet brightness is enormous, as predicted in Section 2, and as we shall see in Section 4.

3.3. Aspects of the Scattering Function

3.3.1. "Scattering" vs. "Phase" Function: What's in a Name?

We deliberately refer to $\Phi(\theta)$ as the "scattering", rather than the "phase", function of the coma, and use the scattering angle, θ, rather than the phase angle, β (see Fig. 2), as its parameter. This is contrary to the usual astronomical convention — for example, the use of β in ephemerides published in publications of the *ICQ*, the Central Bureau for Astronomical Telegrams, and the Minor Planet Center. My choices conform better to the nomenclature in the light-scattering literature of Section 2.3, which by its own convention generally describes "scattering" (and not "phase") functions parameterized by θ (and not β). The choices also underscore the radically different physical optics underlying the brightness behavior of large, solid objects like the moon and major/minor planets on the one hand, and dispersed microscopic comet dust on the other. The behavior of the former generally depends on the illuminated fraction ("phase") and large-scale shadowing effects, while that of the latter depends on small-scale scattering and diffraction effects on the order of a wavelength of light. Thus, cometary coma-brightness behavior is nothing at all like "phases of the moon". Near inferior conjunction, the moon appears extremely dim, while a comet appears overwhelmingly bright. The fog example in Figure 1 illustrates this distinction: In the left panel, the fog is dim and the ground is brighter away from the sun; toward the sun (right panel), the fog is bright and the ground is dimmer.

3.3.2. Relation to Geometric Albedo

$\Phi(\theta)$ is directly related to the grain's geometric albedo as $A_g(\theta) = A_g(180°)\Phi(\theta)$, where $A_g(180°)$ is the ratio of the energy scattered at $\theta = 180°$ to that scattered by a white (completely unabsorptive) Lambert disk of the same geometric cross section as that of the grain (Hanner *et al.* 1981). $A_g(\theta)$ is typically quite low, ≈ 0.05 at $\theta = 180°$ and ≈ 0.025 at side-scattering angles (Kolokolova *et al.* 2004a), but can exceed 1 in forward-scattering regimes. *Bond* albedo (Sec. 3.3.3) and *bolometric* albedo (Sec. 4), on the other hand, can never exceed 1.

3.3.3. The Dark Side of Forward Scattering

Cometary nuclei are the blackest bodies in the solar system. The optical reflectivities of those directly imaged by spacecraft — 1P/Halley, 19P/Borrelly, 81P/Wild, and 9P/Tempel — are all less than 5-6 percent (Weaver 2004; A'Hearn *et al.* 2005). The Bond albedo[3] of 19P, 0.009 ± 0.002, is the lowest measured for any solar-system object (Buratti *et al.* 2004). These findings refute earlier notions of comets as snowy and bright. Greenberg (1986) correctly predicted that comets would be dark. He reasoned that the tiny grains at the nucleus' surface would strongly forward-scatter sunlight into the nucleus, increasing the chances for its absorption after multiple scattering events. In effect, cometary nuclei become light traps, and thus, very black. While cometary darkness must be due to absorption in large measure, Greenberg (1986) argues that cometary nuclei are especially black for the very reason that their comae are so bright at small θ: forward scattering.

3.4. Modeling the Dust Scattering Function, $D(\theta)$

3.4.1. The Henyey-Greenstein Function

Van de Hulst (1980) lists, in his Table 10.1, the many mathematical approximations available for the angle-dependent scattering behavior of small particles. Of these, none has been so successful or widely applied as the Henyey-Greenstein (HG) function. Louis G. Henyey (1910-1970) and Jessie L. Greenstein (1909-2001) devised it while at Yerkes Observatory to analyze diffuse, scattered, galactic radiation (which they found to be "strongly forward-throwing"), and noted that their functions "resemble those computed on the basis of Mie theory for particles whose radius is near a wave length" (Henyey and Greenstein 1941). HG functions subsequently have been applied to model forward-scattering in astrophysical and non-astrophysical environments as diverse as the interstellar medium (*e.g.*, Draine 2003); the Pleiades reflection nebula (Gibson and Nordsieck 2003); dusty spiral galaxies (Bianchi *et al.* 1996); supernovae and their light echoes (Patat 2005); circumstellar-dust disks such as that of β Pictoris (e.g., Kalas and Jewitt 1995); the zodiacal-dust band (Hong 1985); a putative Martian ring (Błecka and Jurewicz 1998); the atmospheres of Mars (Thorpe 1981), Jupiter (Muñoz *et al.* 1999), and Saturn (*e.g.*, Tomasko *et al.* 1980); and seawater (Haltrin 2002). Given its wide application in astrophysics, it is

[2]The potential artifactual underestimation of the size and magnitude of the coma due to its effective magnification by near-earth distance, Δ. A "delta effect" would produce $k < 2$ in a light-curve analysis (see, *e.g.*, Jewitt 1991).

[3]The fraction of incident light that is reflected and refracted, but not diffracted (Hanner *et al.* 1981).

astonishing that the HG function has not hitherto been applied to comets. Here we apply the HG function to model comet brightness for the first time.

The HG function is defined (Henyey and Greenstein 1941) as

$$p_{HG}(\theta, g) = \frac{1}{4\pi} \frac{1 - g^2}{(1 + g^2 - 2g\cos\theta)^{3/2}}, \tag{11}$$

where θ is the scattering angle and

$$g = 2\pi \int_{-\pi}^{+\pi} p_{HG}(\theta, g) \cos\theta \sin\theta d\theta = \langle \cos\theta \rangle \tag{12}$$

is the "asymmetry factor", equal to the mean cosine of the scattering angle of a set of single-scattering events[4]; g ranges from -1 to $+1$. If $g = 0$, $p_{HG}(\theta, 0)$ is flat at $1/(4\pi)$; in this case only, $p_{HG}(\theta, 0)$ does not increase toward 0° or 180°. If $g > 0$, $p_{HG}(\theta, g)$ is forward-throwing — *i.e.*, increases toward $\theta = 0°$. If $g < 0$, $p_{HG}(\theta, g)$ is backward-throwing — *i.e.*, increases toward $\theta = 180°$. These properties are illustrated for different values of g in Figure 11. In this figure, we see that as $|g| \to 1$, $p_{HG}(\theta, g)$ becomes more steeply and narrowly forward-throwing or backward-throwing. A notable and handy property of $p_{HG}(\theta, g)$ is that g parses the modeled scattered flux equally so that half the flux falls within $\langle\theta\rangle = \cos^{-1} g$.

◇ ◇ ◇

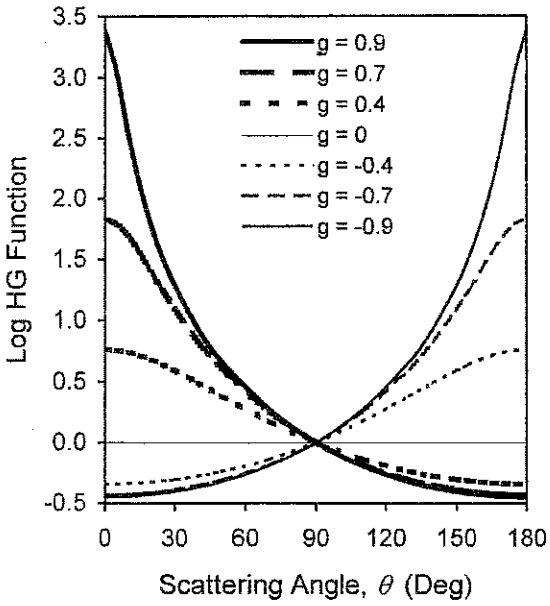

Figure 11. The Henyey-Greenstein function. Positive values of the asymmetry factor, g, give forward-scattering, negative values give back-scattering, and at g = 0 the function is flat. Half the modeled flux falls within $\langle\theta\rangle = \cos^{-1} g$. For the positive g values illustrated in this figure, the corresponding $\langle\theta\rangle$ values are 25°.8 for 0.9, 45°.6 for 0.7, 66°.4 for 0.4, and 90° for 0. The functions are normalized to $\theta = 90°$ by Equation 14.

◇ ◇ ◇

The function $p_{HG}(\theta, g)$ is normalized by default so that the flux integrated over a whole sphere is

$$2\pi \int_0^{\pi} p_{HG}(\theta, g) \sin\theta d\theta = 1 \tag{13}$$

The modeled flux is thus conserved (scattered radiation cannot exceed incident radiation), and no matter how extremely amplified, the forward-scattered flux cannot be infinite for $-1 < g < +1$.

To stick with our adopted convention (Equations 5-8), we normalize the Henyey-Greenstein function of Equation 11 to $\theta = 90°$:

$$P_{HG}(\theta, g) = \frac{p_{HG}(\theta, g)}{p_{HG}(90°, g)} = \left[\frac{1 + g^2}{1 + g^2 - 2g\cos\theta}\right]^{3/2}. \tag{14}$$

[4]Implicitly, there are numerous photons that are scattered, so that g defines their mean direction; this is the nomenclature used in the "scattering" literature. A given photon is assumed to be scattered just once, not multiple times, since we're dealing with an optically thin dust coma.

This action re-normalizes Equation 13 to $1/p_{\rm HG}(\theta, g) = 4\pi(1+g^2)^{3/2}/(1-g^2)$. Note that the functions displayed in Figure 11 are normalized to 90° by Equation 14.

The Henyey-Greenstein function is heuristic, lacking a direct physical basis. Indirectly, the g parameter relates to effective particle size. Higher values indicate larger sizes — a property that will prove handy in modeling actual cometary forward-scattering behavior in Section 4. Desirably, the function is a conservative one that, if it errs, may slightly underestimate the true extent of forward scattering in astrophysical environments (Bianchi *et al.* 1996; Patat 2005).

3.4.2. The Dust-Scattering Function as a Compound Henyey-Greenstein Function

We know that the dust-scattering function, $D(\theta)$, must consist of *both* a forward-scattering and a back-scattering component. Building with Equation 14, we can accordingly model $D(\theta)$ as a *compound* Henyey-Greenstein function of the form

$$D_{\rm HG}(\theta, g) = kP_{\rm HG}(\theta, g_f) + (1-k)P_{\rm HG}(\theta, g_b), \tag{15}$$

where $g_f = \langle \cos\theta_f \rangle \geq 0$ and $g_b = \langle \cos\theta_b \rangle \leq 0$ are the asymmetry factors for the forward- and backward-scattering components, respectively. The $D(\theta)$ term of Equations 5 and 8 has been given an 'HG' subscript here to indicate that this is no longer an "observed" function, but is now simulated. The variable $0 \leq k \leq 1$ is a "partitioning coefficient". In our applications, k is near 1, giving the $P_{\rm HG}(\theta, g_f)$ term more weight, because forward scattering is so much stronger than back scattering in comets, as we shall see in Section 4. Note that Equation 15 remains normalized at $\theta = 90°$ because its components, $P_{\rm HG}(\theta, g_f)$ and $P_{\rm HG}(\theta, g_b)$, are so normalized, and the sum of the coefficients k and $1-k$ is 1.

◇ ◇ ◇

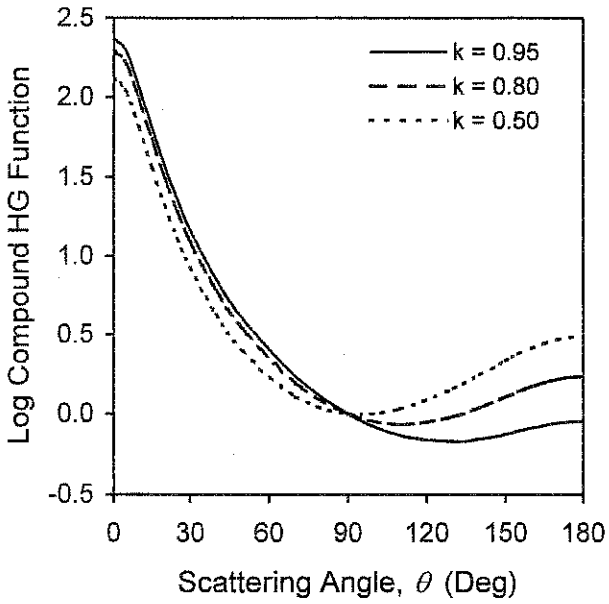

Figure 12. Compound Henyey-Greenstein function for different partitioning coefficients k (see text). Forward-scattering and back-scattering asymmetry factors in this example are $g_f = 0.8$ and $g_b = -0.4$, respectively. Normalized to $\theta = 90°$.

◇ ◇ ◇

Figure 12 shows examples of compound-HG functions with $g_f = 0.8$ (strongly forward-throwing), $g_b = -0.4$ (moderately backward-throwing), and different values of k. The two components have relatively little effect on one another in the simulated forward-scattering and back-scattering regimes because the values of each are relatively low in the other's territory, as is evident from Figure 11. On the other hand, the rises in the two components approximately cancel each other in the mid-scattering regime ($\approx 80° \leq \theta \leq \approx 150°$) when $k \approx 0.95$, so that the compound function is flattened, as we should expect for the true scattering function. This realistic flattening effect can be satisfactorily achieved with just two HG functions, although some modelers prefer to use three. With the chosen values of $g_f = 0.8$ and $g_b = -0.4$, the modeled $D_{\rm HG}(\theta)$ functions in Figure 12 simulate rather well the dust-scattering functions in Figures 8 and 9. Those in Figure 10 are more forward-throwing and would require higher model-g_f values.

3.5. Modeling the Dust-to-Gas Light Ratio, δ_{90}, for Visual Observations

As we have noted, δ_{90} (Equations 6 and 8) is passband-dependent. In this section, we examine δ_{90} specifically as perceived by human scotopic vision. This passband is important, for it comprises the bulk of observations published in

the *ICQ*, and it is the one that we shall use to model forward-scattering observations in historical cometary apparitions in subsequent papers in this series. Note that visual is not the passband of the forward-scattering observations that we shall analyze in Section 4 (those data were generally taken in deeper wavebands that emphasized red and infrared wavelengths). We distinguish δ_{90}, the dust-to-gas *light* ratio, from the dust-to-gas *mass* ratio (*e.g.*, Lara *et al.* 2004) or dust-to-gas *production-rate* ratio (*e.g.*, Storrs *et al.* 1992; A'Hearn *et al.* 1995). These latter can serve as proxies for δ_{90}, but they do not as directly relate to the visual impression.

The ratio δ_{90} varies both with distance from the nucleus and with heliocentric distance. In the Newburn (1981) model, at $r = 1$ AU, δ_{90} is about 1.3 at 25000 to 120000 km from the cometary nucleus, but considerably higher closer in, where the dust is being produced. Early data had indicated that δ_{90} is small near the sun and large away from it. From his sample of comets, Newburn (1981, 1984) obtained $\delta_{90}(r) = 0.416r^2$ for $r < 1.25$ AU and $0.333r^3$ for $r > 1.25$ AU. This formula would give $\delta_{90} = 0.004$ if extrapolated to 0.1 AU, 0.4 at 1 AU, and 3 at 3 AU. From their set of comets, de Almeida *et al.* (1997) found a similar trend with r: $\delta_{90}(r) = (0.61 \pm 0.25)r^{1.8\pm0.5}$ for 0.5 AU $< r <$ 2.5 AU, which gives $\delta_{90} = 0.18$ at 0.5 AU, 0.61 at 1 AU, and 3.2 at 2.5 AU.

The reality of the trend for low δ_{90} at small r is questionable, however, for a number of reasons:

1) The dispersions in $\delta_{90}(r)$ in the Newburn (1981, 1984) and de Almeida *et al.* (1997) data sets are wide, about 1 log, which lessens the statistical determinacy of solutions.
2) Compounding this, in neither data set is there a good statistical representation of comets at $r < 1$ AU.
3) More importantly, it is now clearer that those few comets represented at $r < 1$ AU are statistical *outliers* with uncharacteristically low δ_{90}, 0.13 in the case of 2P/Encke (Newburn 1981). They are among the gassiest of the 85 comets in the massive study of A'Hearn *et al.* (1995). Specifically, at $r < 1.2$ AU, the Newburn (1984) data set is dominated by 2P/Encke and 9P/Tuttle, which have among the lowest dust-to-gas production-rate ratios in the study by A'Hearn *et al.* 1995. The same is true of the extremely gassy comets C/1979 Y1 (A'Hearn *et al.* 1981), 23P/Brorsen-Metcalf, and 2P/Encke, which exclusively represent the de Almeida *et al.* (1997) data at $r < 0.8$ AU.
4) There are strong arguments that, for most comets, $\delta_{90}(r)$ should *increase* at small heliocentric distances. Grynko *et al.* (2004) reason that, because the destruction scale-length of C_2 — the major contributor to visible gas emission — follows an r^2 law, the coma light at decreasing small r should be increasingly dominated by dust as the C_2 coma shrivels. Likewise, Kimura *et al.* (2002) note that at r $\ll$ 1 AU, the light of Kreutz sungrazing comets comes from radiation scattered by dust "to a large extent".

These arguments on the behavior of δ_{90} at small r are important for our model, for forward-scattering can occur only when comets are at $r \lesssim 1$ AU for observers on earth (Fig. 2). In contrast to the situation for $r < 1$ AU, the observed increase in $\delta_{90}(r)$ at $r > 1$ AU appears secure; it is corroborated by A'Hearn *et al.* (1995), who find that the ratio of dust to OH gas production, $Af\rho/Q(\mathrm{OH})$, increases with r, although scaling only as $r^{1/2}$, a more shallow r-dependence than for $\delta_{90}(r)$ in the Newburn (1981, 1984) and de Almeida *et al.* (1997) studies mentioned above. Even in the large A'Hearn *et al.* (1995) data set, there are no data points for $r < 0.5$ AU, and very few for 0.5 AU $< r <$ 1.0 AU, so the behavior of $Af\rho/Q(\mathrm{OH})$ at $r < 1$ AU is not well determined. A'Hearn *et al.* (1995) also find a wide geometric dispersion, about 1.4 log, in the $Af\rho/Q(\mathrm{OH})$ ratio.

With the above considerations in mind, we propose here that the dust-to-gas light ratio is realistically approximated by

$$\delta_{90}(r) = \frac{r^{-1} + r^2}{2}. \tag{16}$$

This formula gives $\delta_{90}(r) \approx$ 1-1.5 over 0.4-1.5 AU, very close to the values remaining in the Newburn (1981, 1984) and de Almeida *et al.* (1997) data sets after the "outlier" comets are rejected. It accepts the Grynko *et al.* (2004) argument that $\delta_{90}(r)$ should increase when r falls much below 1 AU, giving $\delta_{90}(r) = 5$ at 0.1 AU. And as r increases beyond 1 AU, it replicates the increase in $\delta_{90}(r)$ expected in all three data sets cited here, giving $\delta_{90}(r) = 3.3$ at 2.5 AU. However, given the large dispersion in data points at any r, Equation 16 and any formula for $\delta_{90}(r)$ must be taken with "a large grain of salt". For the human visual scotopic passband, a simple, reasonable, and conservative default assumption is to set $\delta_{90}(r) = 1$ for $r < 1$ AU and recognize that statistically some 80-90 percent of comets will fall within 1 log — *i.e.*, $0.3 < \delta_{90}(r) < 3$.

3.6. Folding in the Dust-to-Gas Light Ratio

Figure 13 shows the result of folding in different values of δ_{90} with $D_{\mathrm{HG}}(\theta)$ to obtain $\Phi_{\mathrm{HG}}(\theta)$, the ultimate model of the cometary scattering function, $\Phi(\theta)$ [see Equation 8]. Again, the 'HG' subscripts indicate that $D_{\mathrm{HG}}(\theta)$ and $\Phi_{\mathrm{HG}}(\theta)$ are simulations using Henyey-Greenstein functions. In this example, we use forward- and backward-scattering asymmetry factors $g_f = 0.9$ and $g_b = -0.6$ for $D_{\mathrm{HG}}(\theta)$, and a partitioning coefficient of $k = 0.95$. These values best fit the scattering data on comets that will be presented in Sections 4.2 and 4.4. As Figure 13 shows, decreasing the dust-to-gas ratio delays and blunts the increases in $\Phi_{\mathrm{HG}}(\theta)$ as $\theta \to 0°$ and as $\theta \to 180°$ and flattens the function in the side-scattering regime. At $\delta_{90} = 1$ — the value that is best-suited for the human eye's visual passband (Sec. 3.5) — the modeled forward-scattering enhancement at $\theta = 0°$ compared to 90° is 3.0 log = 7.5 mag = 1000-fold. As δ_{90} increases from a very gassy 0.1 to a very dusty 10, the enhancement increases ten-fold, from 2.32 log = 5.8 mag = 210-fold to 3.32 log = 8.3 mag = 2100-fold (see Fig. 13). Note that the model curves are not very sensitive to differences in particular values of high dust-to-gas ratios. The curve for $\delta_{90} = 3$ is very close to that for $\delta_{90} = 10$, and the $\delta_{90} = 10$ curve would be essentially the same as that for $\delta_{90} = \infty$ (not shown).

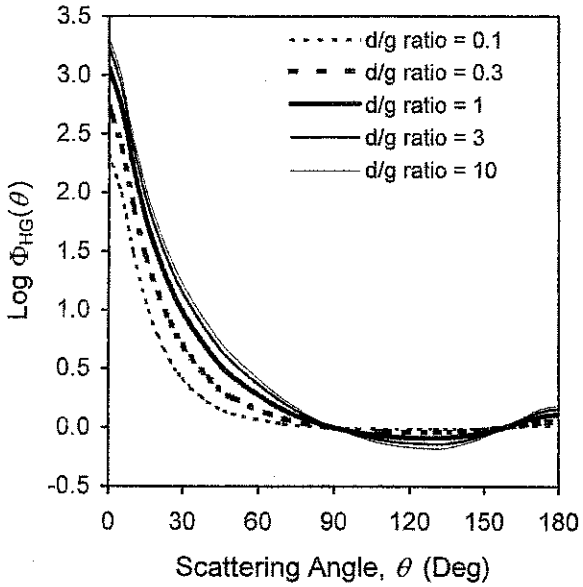

Figure 13. Model for the cometary scattering function, $\Phi_{HG}(\theta)$, for different dust-to-gas light ratios, δ_{90}. The parameters for the underlying compound Henyey-Greenstein function are $g_f = 0.9$, $g_b = -0.6$, and $k = 0.95$. Note that smaller values of δ_{90} blunt and narrow the forward- and back-scattering peaks and flatten out the function at the intermediate angles ($90° < \theta < 150°$) at which comets are most-often observed. Normalized to $\theta = 90°$.

◇ ◇ ◇

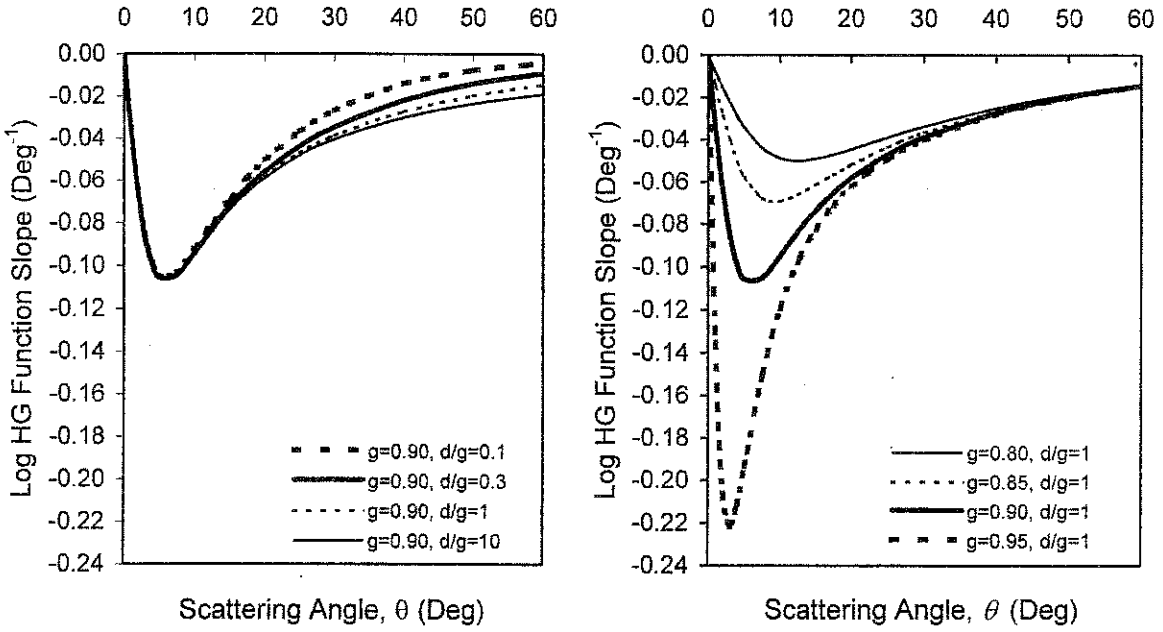

Figure 14. The slopes of the cometary scattering function, log $\Phi(\theta)$, in the forward-scattering regime are shown for different values of the asymmetry parameter g_f and the dust-to-gas ratio δ_{90}. In the left panel, g_f is held constant at 0.90 while δ_{90} varies from 0.1 to 10. In the right panel, δ_{90} is held constant while g_f varies from 0.80 to 0.95. The heavy solid line in each panel represents the default parameters ($g_f = 0.90$, $\delta_{90} = 1$) adopted in this paper for visual observations. Note that δ_{90} controls the slope for $\theta \gtrsim 25°$, while g_f controls it for $\theta \gtrsim 25°$.

◇ ◇ ◇

3.7. The Slope of the Scattering Function in the Forward-Scattering Regime

Because the back-scattering parameter g_b has negligible effect in the forward-scattering regime (see Sec. 3.4.2), we can represent the cometary scattering function, $\Phi(\theta)$, for $\theta \lesssim 60°$ as a *single*-term Henyey-Greenstein function by setting $k = 1$ in Equation 15. Then, from Equations 8 and 14,

$$\Phi_{\rm HG}(\theta) = \frac{\delta_{90}}{1+\delta_{90}}\left[\left(\frac{1+g_f^2}{1+g_f^2-2g_f\cos\theta}\right)^{3/2} + \frac{1}{\delta_{90}}\right]. \quad (17)$$

The slope of this function in the forward-scattering regime contains useful information about the asymmetry factor, g_f, and the dust-to-gas light ratio, δ_{90}. It can be derived by differentiation with respect to θ: Because our convention has been to plot $\Phi(\theta)$ as a logarithm in the figures in this paper, we differentiate it in logarithmic form to obtain

$$\frac{d}{d\theta}\log\Phi_{\rm HG}(\theta) = \frac{-3(\log_{10}e)g_f(1+g_f^2)^{3/2}(1+g_f^2-2g_f\cos\theta)^{-5/2}\sin\theta}{\left(\frac{1+g_f^2}{1+g_f^2-2g_f\cos\theta}\right)^{3/2}+\frac{1}{\delta_{90}}}, \quad (18)$$

where $e = 2.718...$ is the base of natural logarithms. The unit of the slope is rad^{-1}, which can be converted to degrees^{-1} via multiplication by $180°/\pi$.

Figure 14 plots the slopes of the modelled scattering function, log $\Phi_{\rm HG}(\theta)$, for values of g_f and δ_{90} that may reasonably be expected for comets. Note that for $\theta \gtrsim 25°$, the slope is influenced mainly by δ_{90}, while for $\theta \lesssim 25°$, it is influenced mainly by g_f. These two properties will be useful to keep in mind as we fit actual comet scattering data to the Henyey-Greenstein model in Section 4.3.

4. Application of the Model to Comets

4.1. The Detection of Scattering Brightness Enhancement in Comets

Forward-scattering brightness enhancement can be detected in a number of ways, qualitative and quantitative (Marcus and Seargent 1986). Qualitatively, a comet may become unexpectedly visible in twilight or in daylight in forward-scattering geometry. Conversely, it may dim unexpectedly fast as it exits forward-scattering geometry. Forward scattering can enhance the dust continuum of the comet's spectrum relative to the emission lines (Vanýsek 1968). This spectral change occurred in C/1927 X1 (Skjellerup-Maristany) and several other comets that entered forward-scattering geometry (Marcus and Seargent 1986). Spectrophotometry can quantify such changes, as it has done for comets that have entered back-scattering geometry (see Sec. 4.4).

A comet's light curve, $I(\theta, r, t)$, can be used to derive a scattering function (cf. equation 8) as

$$\Phi(\theta) = \frac{I(\theta, r, t)}{I(\theta_0, r_0, t_0)}, \quad (19)$$

where $I(\theta_0, r_0, t_0)$ is a reference brightness at a chosen scattering angle, θ_0, and corresponding heliocentric distance, r_0, and time, t_0. A major disadvantage of this method is that the brightness is dependent not only upon θ, but upon the confounding variables of time, t, and/or heliocentric distance, r. These other dependencies [5] can introduce very significant uncertainties and errors in the forms of short-term and long-term time-dependent variations in $I(\theta)$ and departures from the r^{-n} power law of Equations 9-10.

The "gold standard" for obtaining $\Phi(\theta)$ is visible/infrared photometry. Grains in the coma scatter sunlight in the visible and near-infrared, and re-emit the absorbed component as heat in the deeper infrared. Being very small, comet grains are in essentially instantaneous steady-state thermal equilibrium (Gehrz and Ney 1992) — so that at any time, what they absorb equals what they emit. Because the grains are in steady-state equilibrium, the energy balance in the coma can be characterized by the ratio

$$\mathcal{R}(\theta) = \frac{f_{\rm s}(\theta)}{f_{\rm t}}, \quad (20)$$

where $f_{\rm s}(\theta)$ is the power of the flux in the visible and near-infrared from sunlight scattered off of the dust[6], and $f_{\rm t}$ is the power of the heat flux in the deeper infrared (Ney 1982; Gehrz and Ney 1992; Gehrz 1997). The value of $f_{\rm s}(\theta)$ depends on the scattering angle, but $f_{\rm t}$ does not, because heat radiates isotropically. For a given type of dust in the coma, their ratio $\mathcal{R}(\theta)$ at a given θ remains a constant because both $f_{\rm s}(\theta)$ and $f_{\rm t}$ scale directly to the dust-production rate. $\mathcal{R}(\theta)$ thus is independent of the dust-production rate, and therefore of r and t, as well. The scattering function is related to the energy balance as

$$\Phi(\theta) = \frac{\mathcal{R}(\theta)}{\mathcal{R}(\theta_0)}, \quad (21)$$

[5] A formula incorporating both r and t would be $I = I_0[\Phi(\theta)]r^{-n}S\sin[b+(t-T)/P]$, where the comet's brightness, I, varies periodically over time, t, as a sine function of its rotation period, P, with an amplitude, S, a phase delay, b, and a fixed point in time, T; the brightness also varies with scattering angle, θ, as $\Phi(\theta)$.

[6] $f_{\rm s}(\theta)$ and $f_{\rm t}$ are obtained by fitting blackbody curves to multichannel broadband photometry in visible and infrared wavebands (*e.g.*, Gehrz 1997). Because the V band is sometimes used to derive the $f_{\rm s}(\theta)$ curve, some emission-line contamination (particularly from C_2) may be expected in these measures of $\mathcal{R}(\theta)$.

where θ_0 is a reference scattering angle, which by convention we prefer to set to 90° when possible. Because $\mathcal{R}(\theta)$ is independent of r and t, $\Phi(\theta)$ as expressed in Equation 21 is also independent of r and t, which is a distinct advantage over the variant formulation of $\Phi(\theta)$ in Equation 19.

$\mathcal{R}(\theta)$ is related to the bolometric albedo[7] (Hanner *et al.* 1981; Gehrz and Ney 1992; Gehrz 1997) as

$$A(\theta) = \frac{\mathcal{R}(\theta)}{1+\mathcal{R}(\theta)}. \tag{22}$$

Inasmuch as there may be some gas contribution to the $f_s(\theta)$ of Equation 20, $A(\theta)$ as defined here may to-some-degree overestimate the true grain albedo. In practice, the bolometric albedo for a given scattering angle may differ somewhat from comet to comet. The scattering functions of different comets can be normalized to 90°, as we will do in the next section, by appropriate adjustments of $A(90°)$ for each comet.

4.2. Comets Measured in Forward-Scattering Geometry

Although numerous comets have entered forward-scattering geometry throughout history, only five have been measured in such a way as to allow quantitative scattering functions to be derived. Three of them — C/1927 X1 (Skjellerup-Maristany), C/1975 (West), and C/1980 Y1 (Bradfield) — were analyzed by simultaneous visible-thermal photometry, while the other two — 96P/Machholz (in 2002) and C/2004 F4 (Bradfield) — were recently assayed in the SOHO satellite LASCO C3-coronograph field by visible and near-infrared (non-thermal) photometry. In this section, we present these data and show how they fit our compound-HG scattering-function model, using the parameters $g_f = 0.9$, $g_b = -0.6$, $k = 0.95$, and $\delta_{90} = 10$, obtained through least-squares fitting.

4.2.1. Comet C/1927 X1 (Skjellerup-Maristany)

This comet blazed unexpectedly into naked-eye daylight visibility several degrees from the sun, deep in forward-scattering geometry, reaching a minimum scattering angle $\theta_{\min} = 6°.5$ on 1927 Dec. 15.4 UT and perihelion on $T =$ Dec. 18.2 at $q = 0.176$ AU. Details of its remarkable daylight apparition will be provided in a subsequent paper of this series. At Lowell Observatory in Flagstaff, Arizona, Carl O. Lampland (1873-1951) measured the comet in broad daylight on four consecutive days beginning on 1927 Dec. 16, using a radiometer attached to the 102-cm reflector (Lampland 1928). This extraordinary feat represents the first infrared observations ever of a comet. Because he reported his observations only as a rough abstract (Lampland 1928) and never published a formal paper,[8] Lampland's achievement essentially faded from collective memory by the late-20th century, although we have been reminded of it by Hoag (1984) and Yeomans (1991). Recently I reduced Lampland's observations, which are recorded in his logbooks in the archives of Lowell Observatory (Marcus 2004). I used a model for the comet's visible and thermal spectra and the transmissivities of Lampland's filter screens (water cell, pyrex glass, and quartz), the atmosphere, the telescope optics, and the radiometer thermocouple to obtain preliminary mean values of $\mathcal{R}(\theta)$ on Dec. 17.0 ($\theta = 30°.3$), 17.9 ($\theta = 49°.8$), 18.9 ($\theta = 70°.1$), and 19.9 UT ($\theta = 88°.6$). I plot these data points as log $\Phi(\theta)$ in Figure 15; they have been least-squares fitted to the normalized, compound-HG-function model, which requires $A(90°) = 0.19$ (cf. Equations 21 and 22). I have subsequently obtained an unpublished transmission curve for an additional filter that Lampland used (a microscope cover glass), which will allow those filtered observations to be added in the final data reduction that is now underway (Marcus 2007a).

4.2.2. Comet C/1975 V1 (West)

This magnificent comet likewise was visible in daylight by naked eye, although barely so, when in forward-scattering geometry on 1976 Feb. 25.9 UT at $r = 0.199$ AU and $\theta = 38°$, ten minutes before sunset, at $m_1 = -3$ (Bortle 1976). On Feb. 27.2 UT, $\theta_{\min}$ was 32°.1. The comet's nucleus split into four fragments beginning near the time of perihelion on Feb. 25, the same time that the comet was in forward-scattering geometry. The resulting release of dust increased the comet's brightness substantially (in addition to forward scattering), which would immensely complicate any attempt to derive the scattering function from just visible-light photometry and Equation 19. Fortunately, E. Ney and K. Merrill at the University of Minnesota were doing extensive visible/infrared photometry on the comet during this period, so the scattering function could be well-determined from Equation 21. Their seminal paper (Ney and Merrill 1976) firmly established the forward-scattering character of micron-size comet dust. Their data (Ney 1982; Gehrz and Ney 1992) are plotted in Figure 15, where I have least-squares-fitted them to the normalized-HG-function model by setting $A(90°) = 0.15$ (cf. Equations 21 and 22).

4.2.3. Comet C/1980 Y1 (Bradfield)

This comet was intrinsically fainter and much-less-widely observed than was C/1975 V1. It reached perihelion on $T =$ 1980 Dec. 29.5 UT at $q = 0.260$ AU and $\theta_{\min} = 14°.1$ on Dec. 30.8 UT. Its scattering function in Figure 15 is based on data in Ney (1982) and in Gehrz and Ney (1992), which I have least-squares-fitted to the normalized compound-HG-function model by setting $A(90°) = 0.15$ (cf. Equations 21 and 22).

---

[7] The ratio of the light scattered by the grains to that absorbed and re-emitted at a given scatter angle. The mean bolometric albedo averaged over all θ is $\frac{1}{\pi}\int_0^\pi A(\theta)d\theta$.

[8] Tenn (2007) notes that Lampland, "a scholar and a perfectionist" who worked at Lowell Observatory from 1902 to 1951, unfortunately "hardly ever found his results sufficiently perfect to publish".

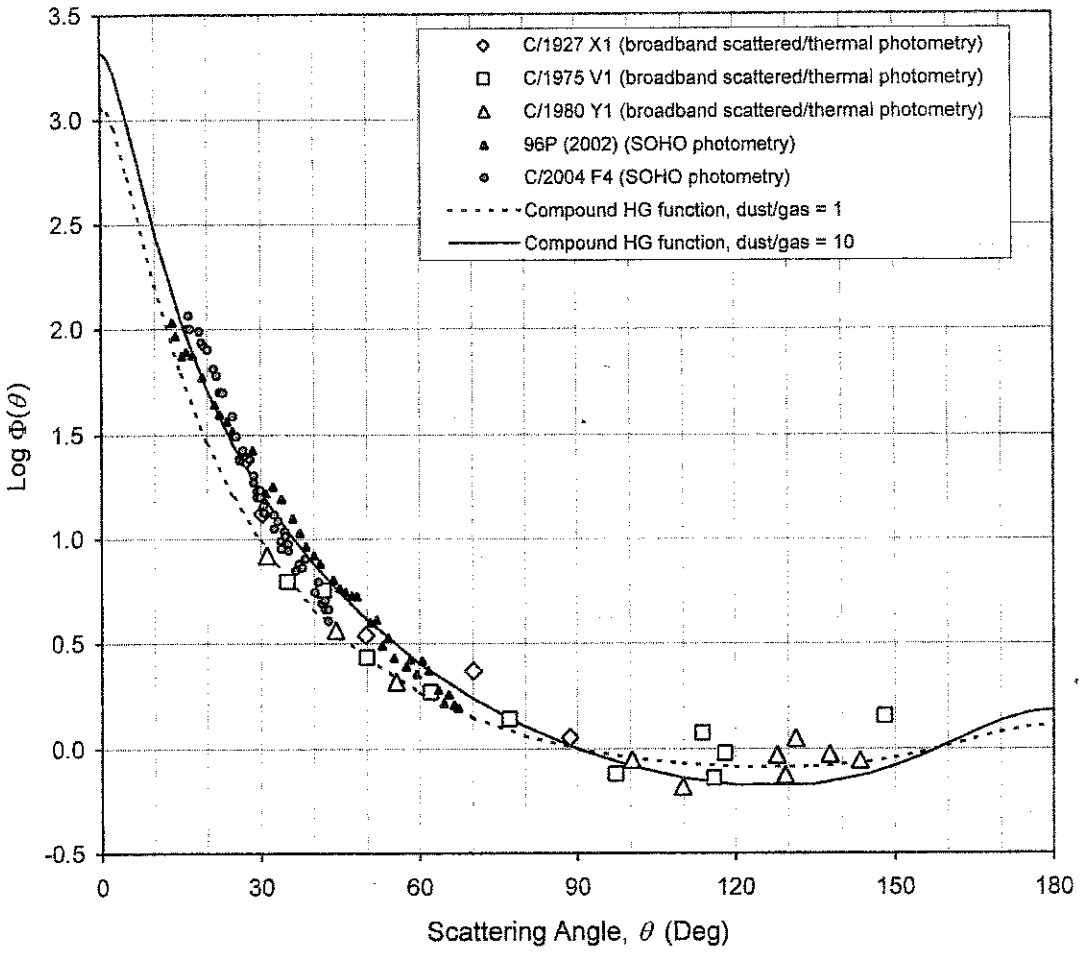

Figure 15. Forward-scattering in comets. Plotted are the five comets measured to date in forward-scattering geometry (see Sec. 4.2). Note the 2-log = 5-mag = 100-fold brightness enhancement by $\theta = 13°.5$, the smallest angle yet measured. The data are fitted by least squares to a compound Henyey-Greenstein function (Equations 8, 14, and 15), normalized to $\theta = 90°$, employing the parameters $g_f = 0.9$, $g_b = -0.6$, $k = 0.95$, and $\delta_{90} = 10$ (solid line). For comparison, a model curve is shown for $\delta_{90} = 1$ (dashed line), which would be appropriate for the human visual passband.

◇ ◇ ◇

4.2.4. Comet 96P/Machholz (in 2002)

This intrinsically-very-faint-but-important short-period comet has a long and durable orbit history (Green *et al.* 1990) and has recently been linked to the Marsden and Kracht "sunskirting" comet groups and the Daytime Arietid and Southern δ Aquarid meteroid swarms (Sekanina and Chodas 2005). The comet flared stupendously while in forward-scattering geometry as it traversed the SOHO satellite C3 coronograph field in 2002 near its perihelion (T = 2002 Jan. 8.6 UT, $q = 0.124$ AU). On Jan. 8.4 UT, $\theta_{\min}$ was 13°.1. The clear-filter images give the most complete coverage, ranging over $13°.5 \leq \theta \leq 67°.3$ and 0.124 AU $\leq r \leq$ 0.152 AU. Grynko *et al.* (2004) analyzed these to derive brightnesses and the comet's scattering function. Because the comet was not at constant r, the authors assumed that the heliocentric magnitude varied by the non-linear empirical formula $H = 12.20 + 12.91 \log r + 6.3 (\log r)^2$, which was proposed early on by Sekanina *et al.* (1990), based on observations from 1986. This law gives a very shallow dependence in the above r range, amounting to only a 0.22-magnitude falloff post-perihelion, equivalent to $n = 1$ in Equations 9 and 10. However, with an absence then of observations at $\log r < -0.18$, the Sekanina *et al.* formula at perihelion ($\log q = -0.91$) represents a huge and uncertain extrapolation.

Subsequently there have been additional m_1 observations in the 1991, 1996, and 2002 apparitions, including two observations near perihelion in 1996 measured from the SOHO-satellite images. Therefore I analyzed the two SOHO estimates and all the visual m_1 estimates from 1986 to 2002 published in the *ICQ* (**8**:46 and 89, 1986; **13**:165-166, 1991; **19**:214, 1997; **24**:22, 2002), correcting the visual ones for magnification artifact with a formula [$-1.25 \log (M/10)$, where the magnification = $M > 10$] that gives a result similar to the Morris "aperture correction" for reflectors (Morris 1973). I find that the comet's composite photometric behavior is essentially linear and well fitted by the least-squares solution $H = 11.1 + 7.3 \log r$ as seen visually at a magnification of 10×. Accordingly, I adjusted the Grynko-*et-al.* brightness data with this better-determined r-dependence to produce the scattering function in Figure 15; its slope over $13°.4 \leq \theta \leq 67°.3$ is slightly more shallow than the slope of Grynko *et al.* (2004), by 0.17 log. I have fitted these data points by

least squares to the normalized compound-HG-function model. The observation at $\theta = 13°.4$ is the smallest scattering angle at which any comet has been measured to date.

4.2.5. Comet C/2004 F4 (Bradfield)

Scattering data are available online in a Ph.D. thesis (Grynko 2005), but at this writing they have not been formally published. Like 96P, comet C/2004 F4 underwent a tremendous flare in brightness in the SOHO/LASCO C3-coronograph field, which correlated exquisitely with the scattering angle. The comet was in forward-scattering geometry at $\theta < 53°$ throughout its traverse of the 16°-diameter field between 2004 Apr. 15 and 20 UT, reaching perihelion on Apr. 17.1 UT at $q = 0.168$ AU and $\theta = 28°.9$; the minimum scattering angle $\theta_{min} = 15°.5$ on Apr. 18.2 UT at $r = 0.174$ AU. Grynko (2005) has reduced the brightnesses in the clear, blue, orange, deep-red, and near-infrared filtered images to derive the scattering function. The function is compromised pre-θ_{min} by a gap during most of Apr. 17 UT due to pixel saturation (the LASCO team anticipated strong forward scattering, but apparently not this strong), most severely affecting the clear-filter set, as well as by several contaminating outbursts that correlate with synchrones seen later in the dust tail. However, the post-θ_{min} arm of the scattering function is continuous over $15°.5 \leq \theta \leq 42°.8$ and 0.174 AU $\leq r \leq$ 0.212 AU, with the most-usable exposures in the blue and infrared filters, and there were no obvious outbursts. We choose the infrared-filter data set because the light it transmits should be much-less contaminated by emission lines. Figure 15 plots the post-θ_{min} infrared-wavelength scattering function after adjustment for a post-perihelion heliocentric-magnitude dependence of $H = 8.1 + 7.7 \log r$ (Grynko 2005). As with the other comets, the data points are least-squares-adjusted to fit the normalized compound-HG-model curve.

4.3. The Composite Forward-Scattering Function for Comets: An Analysis

Figure 15 documents huge increases in cometary brightness caused by forward scattering of light by dust. From 90° to 13°.5 — the smallest scattering angle at which a comet has yet been measured — there is a collective 2-log = 5-mag = 100-fold brightness enhancement. One log = 2.5 mag = a factor of 10 of this enhancement occurs by $\theta = 30°$, as evidenced by the data on the three comets measured by scattered-light/thermal photometry. In the case of 96P, as θ declines from 67°.3 to 13°.5, the brightness amplifies by nearly 2 log = 100 times.

The reality and universality of the forward-scattering enhancement of comet brightness are compelling in these data. All five comets show it. Yet the comets are heterogeneous. Four are of long orbital period, while 96P is of short period (although not a "classical Jupiter-family" member). C/1980 Y1 is of "IR Type I" (cf. Sec. 2.2.4), while C/1927 X1 and C/1975 V1 are of "IR Type II" (Gehrz and Ney 1992; Marcus 2007a). Spectroscopically, C/1975 V1 is "dusty", while C/1980 Y1 is "gassy", as would be predicted by their "infrared types" (cf. Sec. 2.2.4): by convolving their quantitative spectrograms (Chaubey 1978; Goraya *et al.* 1982) with the human-scotopic visibility function (Cox 2000, p. 118), I find their dust-to-gas light ratios, δ_{90}, to be 2.5 and 0.5, respectively, at intermediate scattering angles and comparable r. The heterogeneity of the five comets notwithstanding, their individual scattering curves are reasonably congruent to a first approximation. This indicates a general consistency in the forward-scattering behavior of comets.

The composite of observations fits the compound-HG-function-scattering model rather well when a dust-to-gas ratio of $\delta_{90} = 10$ is used (the solid line in Fig. 15). We chose a value of $\delta_{90} = 10$ in the figure, but the actual value is rather unimportant, because any $\delta_{90} \gg 3$ produces nearly the same asymptotic curve (cf. Fig. 13 and remarks in Sec. 3.6). The choice of a high value is appropriate, for the photometric methods by which the observations were obtained should theoretically admit little opportunity for gas contamination from emission bands. Specifically, in the case of the SOHO comets, the three major C_2 lines between 0.46 and 0.56 μm (*e.g.*, Goraya *et al.* 1982) would be greatly diluted over the broad span of the clear-filter (0.42-0.88 μm) observations of comet 96P, and only negligible contamination from the CN band at 0.92 μm (Gehrz 1997) would be expected in the infrared-filter (0.82-1.0 μm) observations of comet C/2004 F4. In the case of the comets assayed by broadband scattered-light/thermal photometry, contamination by C_2 emission bands in the V filter (C/1976 V1 and C/1980 Y1) or water-cell (C/1927 X1) observations probably are not important (see Sec. 4.2), although this supposition may not be airtight (see below). For comparison with the $\delta_{90} = 10$ curve, I have also shown the compound-HG-function model with $\delta_{90} = 1$ as a dashed line in Figure 15. As discussed in Sec. 3.5, this δ_{90} value is better-suited for observations made by the human eye or with a V-filtered CCD.

The fit of the observations to the compound-HG-function model is excellent, but not perfect. For one thing, the scattered-light/thermal photometry data points (C/1927 X1, C/1976 V1, C/1980 Y1) in Figure 15 fall slightly below the $\delta_{90} = 10$ model at $\theta < 90°$, and slightly above it at $\theta > 90°$, although only by an average of 0.1 log. We know that in the range $30° \leq \theta \leq 150°$ spanned by these data, the δ_{90} parameter drives the shape of the compound-HG-function model (cf. Sec. 3.7). Thus, this slight misfit could occur if the dust-to-gas ratio in at least some of these data were below the assumed value of $\delta_{90} = 10$. Indeed, the scattered-light/thermal data appear to fit the $\delta_{90} = 1$ curve slightly better than the $\delta_{90} = 10$ curve in Figure 15. As a possible explanation, the V filter was one of several that was used in the fit of the scattered-light blackbody curves for C/1975 V1 and C/1980 Y1 (Ney 1982; Gehrz and Ney 1992). Significant C_2 emission contamination in this filter could result in an overestimation of the $f_s(\theta)$ term in Equation 20 and drive down the apparent dust-to-gas ratio. As we noted above, the spectrum of C/1980 Y1 had very significant C_2 contamination, although that of C/1976 V1 did not. We also know that C_2 bands in the spectrum of C/1927 X1 were strong enough to be observed in bright twilight one week before its perihelion passage (Hartmann 1927).

We can see another slight departure from the model fit in the data for C/2004 F4. The brightness increase with decreasing θ exceeds the slope of the compound-HG-function model. As we noted in Section 3.7, the forward-scattering parameter, g_f, drives the shape of the model curve at smaller scattering angles. A steeper data slope would imply that the value of g_f for the C/2004 F4 data is higher than the 0.90 value that we have adopted. But even extremely high (and unrealistic) $g_f \rightarrow 1$ fails to replicate the high C/2004 F4 slope. Therefore, we suspect that factors *additional* to

pure light-scattering effects could be contributing to the brightness behavior of this comet. Two should be considered:

1) *Uneven dust-production rates.* We know from this comet's tail structure that the nucleus was undergoing dust outbursts (cf. Sec. 4.2.5). Uneven dust production could artifactually increase or decrease the apparent scattering-curve slope in the SOHO photometry. As we have noted (Sec. 4.1), intrinsic time-dependent brightness variability is a principal weakness of any method that seeks to extract scattering data exclusively from the light curve by means of Equation 19. Visible/infrared photometry, which derives the scatter function through Equations 20 and 21, does not suffer this pitfall.
2) *Projection geometry.* Contamination of the SOHO coma photometry by the dust tail could artifactually steepen the scattering slope of C/2004 F4, as well as that of 96P. On small scales ($\lesssim 10^4$ km), particles stream outward from the nucleus in roughly spherical symmetry. But on large scales ($\gtrsim 10^4$ km), both large and small ejected particles stay essentially in the comet-orbit plane, with the larger, slower-moving ones preferentially populating the proximal dust tail. As the orbit plane tilts into the line-of-sight at decreasing scattering angles, relatively more tail particles will fall into the effective detector aperture, scaling roughly as $1/(\sin\theta)$. This effect increases with increasing size of the detector aperture. The equivalent diameters of the aperture diaphragms for the C/1975 V1 and C/1980 Y1 measurements were small, 22″.5 and sometimes less (Gehrz and Ney 1992), and for C/1927 X1, the tiny thermocouple receiver projected only 9″ diameter onto the focal plane (Marcus 2007a). In contrast, the 3-pixel-by-3-pixel box used for the SOHO photometry was much larger: 168″ on a side (Grynko 2005), or 189″ equivalent diameter. For 96P and C/2004 F4, at $\Delta \approx 0.85$ AU (and $\theta_{\min} = 13°.5$ and 15°, respectively), the projection in the 189″ aperture corresponded to distances of $\approx$ 450000-500000 km in the orbit plane. Along this considerable span, there is the potential for the planar proximal dust tail to contaminate and increase the signal of what otherwise would be essentially just the coma when measured in smaller apertures. Such contamination could artifactually steepen the coma scattering slopes of the two SOHO comets.

For $\theta < 13°.5$, the HG-model curve represents an extrapolation for which no data from actual comets are currently available. In this context, however, we believe that the choice of $g_f = 0.90$ is judicious; it delivers a 3.4-log brightness enhancement at $\theta = 0°$, as compared to 90°, which is similar to current models for comet grains as 128- and 256-monomer aggregates (cf. Fig. 10 of Kimura *et al.* 2006; and sections 2.3.1 and 2.3.5 of this paper).

4.4. Side Scattering and Back Scattering

This paper is concerned primarily with forward scattering, but we wish to show that the compound Henyey-Greenstein model presented here also works well in *side*-scattering ($90° \leq \theta \leq 150°$) and *back*-scattering ($150° \leq \theta \leq 180°$) regimes. For side scattering, it delivers the essentially flat curve needed to fit the observations in Figure 15. It is difficult (and not particularly meaningful) to specify a precise minimum in this very broad and shallow midrange. In Figure 15, the observations and the HG function respectively give roughly $\theta = 110°$ and 125°. The only comet for which there is a scattering curve at side angles independent of time and r is 1P/Halley, as observed from the *Vega 2* spacecraft; its data indicate a very shallow minimum at a somewhat uncertain $\theta \approx 100°$ (Krasnopolsky *et al.* 1987).

Back-scattering enhancement ranges up to 1 magnitude or so over side-scattering in most studies (Kiselev and Chernova 1981; Millis *et al.* 1982; A'Hearn *et al.* 1984; Meech and Jewitt 1987; Hanner and Newburn 1989; Schleicher *et al.* 1998; Milani 2005). The comet for which there are the most back-scattering observations is 1P/Halley. From narrowband photometry of the continuum in visible light, Schleicher *et al.* (1998) determined the $Af(\theta)\rho$ parameter (A'Hearn *et al.* 1984), a measure of the dust brightness. After correcting it for pre-perihelion and post-perihelion heliocentric-brightness dependencies, the authors derived a scattering curve extending to $\theta = 178°.5$. These data points are shown in Figure 16 as filled circles, fit by least-squares to our compound-HG-function model (the solid line in the figure). We can see that the 1P/Halley observations are well-fitted by the model. To be sure, there is some dispersion, but we must keep in mind that 1P is a very active comet with irregular activity on short time scales, and that the scale of the log $\Phi(\theta)$ axis is much smaller in this figure than in Figure 15. Note the approximately-0.4-log, or 1-magnitude, rise from the broad minimum at $120° \leq \theta \leq 130°$ to back-scattering at $\theta > 175°$.

Back-scattering is usually modeled as a linear function with phase angle in the form $m_{\Phi(\theta)} = -\gamma\beta = \gamma(180° - \theta)$ over $150° \leq \theta \leq 180°$ (cf. Equation 10). The coefficient, γ, is expressed in mag deg^{-1}. Meech and Jewitt (1987) found $\gamma = 0.018$ for comet 1P over $170° \leq \theta \leq 179°$. However, 1P/Halley's brightness jumpiness on short time scales should generate uncertainty over a θ interval this small. Over a more-determinate range of $150° \leq \theta \leq 180°$, I derive $\gamma = 0.028$ from the larger 1P data set of Schleicher *et al.* (1998). From other authors' continuum spectrophotometry, Meech and Jewitt (1987) derive $\gamma = 0.034$ for 47P/Ashbrook-Jackson in 1977 (Kiselev and Chernova 1981), 0.035 for C/1980 E1 (A'Hearn *et al.* 1984), and 0.020 for 38P/Stephan-Oterma in 1980-1981 (Millis *et al.* 1982). Recently, Milani (2005) reported $\gamma = 0.036$ for C/2002 T7 (LINEAR). From the foregoing values (using $\gamma = 0.028$ for 1P), I find a mean $\gamma = 0.031 \pm 0.006$ (standard deviation). This slope is plotted in Figure 16 as a dashed line over $150° \leq \theta \leq 180°$. We see that there is a close correspondence of the linear model and the compound-HG-function model over this range.

The preceding data reductions all suffer in some degree from the uncertain r and t dependencies that were discussed in Sections 4.1 and 4.3. Unfortunately, "gold standard" scattered-thermal photometry in the back-scattering regime is nearly non-existent and "urgently needed" (Jockers 1997). There are two comets, however, for which scattered/thermal photometry extends to $\theta > 165°$: 67P/Churyumov-Gerasimekno (Hanner *et al.* 1987) and C/1986 P1 (Hanner and Newburn 1989). Using Equations 19 and 20, I converted the published $A(\theta)$ values for these comets to log $\Phi(\theta)$ and plot the data points in Figure 16 as a least-squares fit to the compound-HG-model curve. We see that the scattering functions for these comets increase as θ approaches 180°, are congruent with the 1P data set, and fit the compound-HG-model curve quite satisfactorily.

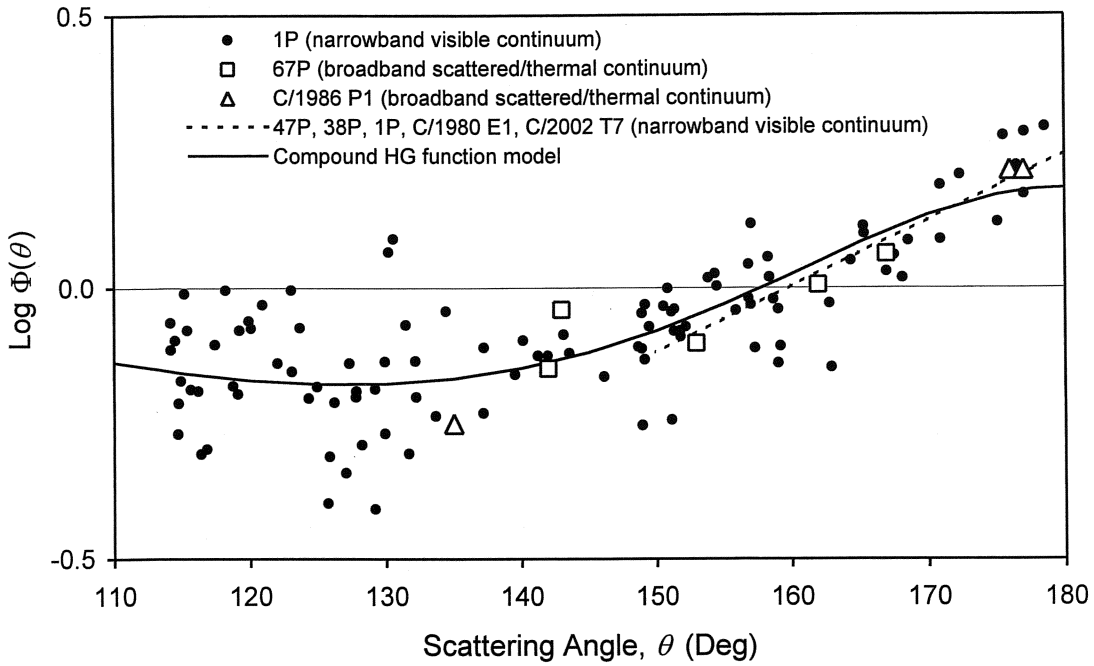

Figure 16. Back-scattering in comets. The data are discussed in Section 4.4. Note the ≈ 0.4-log = 1-mag = 2.5-fold rise in brightness from intermediate to backscattering angles, much less than the rise for forward scattering in Fig. 15. The data are well-fitted by the compound Henyey-Greenstein function (solid line), normalized to $\theta = 90°$, with the same parameters as in Fig. 15. To keep the figure uncluttered, the data for 47P, 38P, 1P, C/1986 E1, and C/2002 T7 are simply represented by their mean slope, 0.031 ± 0.006 mag deg^{-1} (the dashed line), over $150° \leq \theta \leq 180°$.

◇ ◇ ◇

For the HG curve in Figure 16, we assume (as in Figure 15) a dust-to-gas light ratio of $\delta_{90} = 10$ (see caption). In this case, the high value is justified because narrowband spectrophotometry of the dust continuum should have minimal gas-emission band contamination. Likewise, even though the scattered/thermal photometry of 67P and C/1986 P1 is broadband, the scattered light from these two comets was sampled only from J (1.21 μm) and longer-wavelength bands, where gas contamination is minimal. This is in potential distinction to the three forward-scattering comets studied by scattered/thermal photometry in Figure 15, which were sampled in additional shorter-wavelength broadbands, which included V (0.55 μm) data that are prone to gas contamination from C_2 emission (Sec. 4.3). Keep in mind that, for m_1 brightness estimates made with the human eye or via V-filter CCD photometry, the back-scattering curve would look more blunted (see the $\delta_{90} = 1$ curve in Figure 15).

5. Discussion

This paper comprehensively reviews the forward-scattering of sunlight by comets for the first time. After pointing out the ubiquity of forward scattering in diverse environments (Sec. 2.1), we examined the nature of cometary grains, and what theoretical and experimental models say about how they should scatter light (Sections 2.2.3 and 2.3.2). We concluded that *any* comet in which dust contributes significantly to its light — *i.e.*, most comets — *must* display significant forward-scattering brightness enhancement under certain geometrical viewing conditions. As verification, the five comets to date for which there are actual quantitative measures indeed collectively show an approximately-100-fold brightness enhancement by the time θ falls to 13°.5, the smallest scattering angle for which there are data currently (Sec. 4.3). A scattering (or "phase") curve for one of them, the great daylight comet C/1927 X1, was presented here in preliminary form for the first time.

5.1. A Novel "Henyey-Greenstein Function" Model for Comet-Light Scattering

We introduced the Henyey-Greenstein function (Sec. 3.4) to model the scattering curves of comets — the first time that it has been applied to solar-system comets. This was long overdue, for it has been widely used to model dust scattering in other astrophysical environments for over a half century (Sec. 3.1), including the forward-scattering of a putative giant extra-solar sytem comet in the β-Pictoris dust disk (Lamers *et al.* 1997). Folding in the dust-to-gas ratio, δ_{90} (Sections 3.5 and 3.6), we applied the HG function in *compound* form to successfully fit the scattering functions to the five comets that have been measured in forward-scattering geometry (Sections 4.2 and 4.3). We also showed that the same function equally well models side-angle and backward-angle scattering (Sec. 4.4). Thus the model is universal — applicable across all scattering angles — although its application in our study emphasizes forward-scattering. Successful as it is, the HG function is heuristic, and so it should not be over-interpreted. It empirically models the *patterns*, but

not the *physics*, of light-scattering intensity.

Our compound-HG-function model is easy to apply using common personal-computer "spreadsheets" and programmable calculators. As presented here (Equations 8, 14, and 15), it should prove to be a powerful tool for analyzing and forecasting the brightnesses of comets in forward-scattering geometry. As an example, I used the model to successfully predict the 9-fold brightness surge in January 2007 of comet C/2006 P1 (McNaught) to $m_1 \approx -6$, which enabled the comet to become visible to the naked eye in broad daylight (Marcus 2007b, c). Actual comet observations (Sections 4.2-4.4) are well-fitted with parameter values $g_f = 0.9$, $g_b = -0.6$, and $k = 0.95$. While $\delta_{90} \approx 1$ should be used for broadband visible light photometry (m_1 estimates by the human eye and V photometry), $\delta_{90} \approx 10$ is better for narrowband photometry of the continuum and broadband visible/infrared photometry (Sec. 3.5). Of these four parameters, only g_f and δ_{90} are important in the forward-scattering regime ($\theta \lesssim 60°$). In this range, the simplified single-term HG model (Equation 17) can be safely used.

5.2. The Model and the Observations

The fit of our compound-HG-function model to the actual comet observations is excellent on the whole (Figures 15 and 16), although minor departures occur in the forward-scattering regime (Sec. 4.3). In the cases of C/1975 V1 and C/1980 Y1, these could relate to errors in assumed values of the dust-to-gas ratio, δ_{90}. Differences could also be due to the intrinsic form of the HG model itself. Of possible causes, we are the most concerned about the method of extracting the scattering function from observations based on the photometry of *solely* the scattered light (Equation 19). As a critical example, had we not shaved off 0.17 log in the scattering slope of comet 96P/Machholz by the use of an updated light curve that produces a different r-dependence (Sec. 4.2.4), the 96P slope, like that of C/2004 F4, would have been significantly steeper than that of the HG model (Fig. 15). The comparatively larger SOHO diaphragms also could produce artifactually steeper scatter-function slopes for the reasons presented in Section 4.3. With these concerns in mind, the simultaneous photometry of *both* the scattered and thermal fluxes should be considered the "gold standard" method (Equations 20 and 21) for deriving the scattering function, for it is based upon the *ratio* of the scattered and emitted radiation, which is essentially independent of the confounding vagaries of uncertain or unknowable time- and r-dependencies in dust production. Unfortunately, this type of data is not currently available for scattering angles $\theta < 30°$.

Currently we lack direct *quantitative* measures of the scattering-function data for comets at $\theta < 13°.5$. We noted, however, that the compound-HG model, extrapolated to 0° with $g_f = 0.9$ (Fig. 15), fits comet grain-modeling data well (Sec. 4.3). Both the compound-HG model and the grain-modeling data produce a 3- to 3.5-log (1000- to 3000-fold) brightness enhancement at $\theta = 0°$. But how would an actual *comet* behave at this extreme scattering angle? There are direct *qualitative observations* of comets to suggest that such huge enhancements may well occur near 0°. As examples, for C/1927 X1 to have been casually noticed in broad daylight just off the limb of the sun (Goodhue 1928; Bortle 1997a), or for 1P/Halley to have been glimpsed by naked eye in daylight just before transit in 1910 (Marcus 1986; Marcus and Seargent 1986), would require extremely large forward-scattering enhancements of this order. Taking the post-perihelion photometric brightness parameters of 1P/Halley as $m_0 = 3.4$ and $n = 3.0$ (Green and Morris 1987), when this comet reached naked-eye daylight visibility at $\Delta = 0.161$ AU, $r = 0.851$ AU, and $\theta \approx 1°$ on 1910 May 19.2 UT, its *ordinary* brightness, ignoring the scattering function, would have been $m_1 = -1.1$ (Equation 10 with $m_{\Phi(\theta)} = 0$). However, with a 3000-fold brightness enhancement at θ near 0° factored in, $m_{\Phi(\theta)} = -2.5 \log (3000) = -8.7$, and 1P/Halley's brightness becomes $m_1 = -1.1 - -8.7 = -9.8$. This high predicted brightness lends some credence to J. B. Bullock's most unusual daylight report (Marcus 1986). Further, as we saw in Section 2.2.3, the *Giotto*-spacecraft encounter with comet 1P/Halley found $p < 3$ for Equation 1, indicating that most of the dust mass is concentrated in larger grains, more so than for most comets. With larger average particle sizes, the forward-scattering brightness enhancement just off the limb of the sun in 1910 could have been even greater (Sec. 2.3.5).

5.3. Forward-Scattering in Comets: Real, But Little-Recognized

Forward-scattering enhancement of comet brightness has not been widely recognized in the comet-science community, no doubt owing to its rarity as well as to the difficulty in securing observations at the small solar elongations that necessarily attend forward-scattering geometry (Fig. 2). Daylight and twilight snuff out the intrinsically smaller comets before their brightness surges can be detected. For example, the tremendous forward-scattering flares of the small comets 96P and C/2004 F4 in the SOHO C3 coronograph (Sec. 4.2) were unobserved from the earth. But medium- and large-size comets can dramatically pierce through twilight and daylight in forward-scattering geometry, as we will see in some additional examples below. Any comet with visible dust — *i.e.*, essentially *all* comets — will show forward-scattering. Different as they are from each other, all five comets measured to date in forward-scattering geometry not only show forward-scattering brightness enhancement, but roughly the same amounts at comparable scattering angles (Sec. 4.3).

The literature on forward-scattering by real comets (as opposed to models) is sparse, which further accounts for the lack of wider recognition of the phenomenon. Richter (1963) was probably the first to propose that forward-scattering could enhance brightnesses, by factors of 10^3 or even 10^4, citing as an example the brilliant "eclipse comet" C/1948 V1. Later Vanýsek (1968) suggested that forward scattering could be detected as an enhancement in the dust-continuum component of the spectrum. There are positive (Bobrovnikoff 1931) and negative (Howell *et al.* 1991) indications that this occurred in 1P/Halley in 1910, but that comet was in only marginal forward-scattering geometry when the spectra were taken, so the effect would be harder to detect. In stronger forward-scattering geometries, we noted enhanced continua in comets C/1881 K1, C/1874 H1 (Coggia), C/1910 A1 ("Great January Comet"), and C/1927 X1 (Skjellerup-Maristany)

— and that the latter two were also sighted in daylight in strong correlation to small scattering angles (Marcus and Seargent 1986). We suggested that comet 1P/Halley has manifested forward-scattering brightness enhancement in at least several of its historical apparitions, most notably in 1066 when it was reported as "bright" or "big" as the full moon, during 1222 when it was sighted in daylight in Korea, and in 1910 when it was sighted in daylight just before its transit of the sun (Marcus 1986; Marcus and Seargent 1986). Sekanina (1982) invoked forward-scattering to explain the brightening of the surviving tail of C/1979 Q1 (SOLWIND), a Kreutz-sungrazing comet that fell into the sun, and to lend support that its orbit had been retrograde.

We have pointed out that, of the 13 comets of the last two centuries classified as "great" by Bortle (1997a), nine passed nearly between the earth and sun in strong forward-scattering geometry — eight of them at $\theta_{\min} < 25°$, and six at $\theta_{\min} < 14°$ (Marcus 1997). This high incidence is quite remarkable, considering that forward-scattering encounters with comets are relatively rare; it prompted us to suggest that forward-scattering enhancement is a quality that can render comets "great", much as near-sun and near-earth approaches and intrinsic sizes do. Bortle's (1997b) unelaborated skepticism notwithstanding, of those nine comets, forward-scattering exquisitely correlates with and likely accounts for the naked-eye daylight visibilities of C/1861 J1, C/1910 A1, C/1927 X1, and C/1975 V1. The Kreutz-sungrazing comets C/1843 D1, C/1882 R1, and C/1965 S1 (Ikeya-Seki) are more problematic. While their daylight appearances also correlate to forward-scattering geometry, their visibilities must also owe substantially to the r^{-n} brightness law of Equation 9 and these comets' extremely small heliocentric distances (Marcus 1997). We shall look at these and other comets in greater detail in subsequent installments of this series. Bortle's (1976) own remarkable sighting of C/1975 V1 (West) — the last time, before C/2006 P1 (McNaught), that a comet has been reported by naked eye in daylight — is instructive. It came at nearly the same hour that Ney and Merrill (1976) were documenting a 6-fold ($\approx$ 2 mag) enhancement in the scattering function. Had comet C/1975 V1 not enjoyed this brightness "boost" (and been only $m_1 = -1$ instead of $m_1 = -3$), spotting it in daylight near the sun (Sec. 4.2.2) would have been well nigh impossible.

5.4. The Enormous Potential of Forward-Scattering Brightness Enhancement

In his 1906 science fiction novel, *In the Days of the Comet*, H. G. Wells (1924) wrote of a tremendous comet that "looked brighter than the moon because it was smaller, but the shadow it cast, although clearer cut, was much fainter than the moon's shadow. . . . I went on noting these facts, watching my two shadows precede me." With forward-scattering, Wells' scenario is not far-fetched. Using Equation 10, a medium-large comet of $m_0 = 4$ and $n = 4$, passing between the earth and sun at $\Delta = 0.1$ AU, $r = 0.9$ AU, and $\theta = 18°$, would brighten 5.5 mag owing to distance alone, and an additional 1.6 log, or 4.0 mag, based on the scattering function (Fig. 15). Its total magnitude would then be $m_1 = 4 - 5.5 - 4.0 = -5.5$. At some latitude on earth, this comet would hang several degrees above the horizon, casting palpable shadows in deepest twilight. Such a cometary apparition has occurred: During the night of 1861 June 30-July 1, the famed comet observer J. F. Julius Schmidt watched in awe as the great comet C/1861 J1 (Tebbutt) cast shadows on the walls of the Athens Observatory at $\theta = 23°$-$25°$ (Schmidt 1863; Marcus 1997). Another observer in Europe saw the shadows cast by the comet in twilight. (This comet's remarkable forward-scattering light curve will be presented in a subsequent paper.) Now imagine a giant comet of the size of C/1995 O1 (Hale-Bopp), with $m_0 = -1$, grazing the earth at $\Delta = 0.01$ AU, $r = 0.99$ AU, and $\theta = 18°$. From Equation 10, its brightness would be $m_1 = -1 - 10 - 4.5 = -15.5$, over ten times brighter than the full moon! The light from such a comet would overwhelm the full moon's shadows, ruin the observer's dark adaptation, and enable soccer to be played at night.

5.5. Future Directions: The Past

A cometary apparition like the one last described would be very rare, to be sure — an occurrence once in many, many millenia. But comets of lesser extremes have frequently crossed our skies through history. Their mammoth forward-scattering brightenings would have been an unrecognized agent in inspiring the awe and terror of comets recorded by earlier societies. In subsequent articles in this planned series, we shall catalogue the geometric circumstances of forward-scattering encounters of historical comets, and investigate evidence for enhancements of their brightnesses.

Acknowledgements. My investigations into light scattering and comet brightness began with correspondence in the early 1980s with Edward P. Ney (1922-1996), of the University of Minnesota in Minneapolis; to him I am the most indebted. I thank a referee for the careful and detailed critique that was invaluable in improving the paper. I am also grateful for valuable discussions and correspondence with J. Mayo Greenberg (1922-2001), University of Leiden, The Netherlands; Zdenek Sekanina, Jet Propulsion Laboratory, Pasadena, California; Ludmilla Kolokolova, University of Maryland, College Park; and David A. J. Seargent, The Entrance, New South Wales. I thank Naomi Greenberg, Baltimore, for the color copy for Figure 6.

REFERENCES

A'Hearn, M. F. (2006). "Whence Comets?", *Science* **314**, 1708.

A'Hearn, M. F.; M. J. S. Belton; W. A. Delamere; J. Kissel; K. P. Klassen; L. A. McFadden; K. J. Meech; and 26 additional authors (2005). "Deep Impact: Excavating Comet Tempel 1", *Science* **310**, 258.

A'Hearn, M. F.; R. L. Millis; and P. V. Birch (1981). "Comet Bradfield (1979 X): The Gassiest Comet", *Astron. J.* **86**, 1559.

A'Hearn, M. F.; R. L. Millis; D. G. Schleicher; D. J. Osip; and P. V. Birch (1995). "The Ensemble Properties of Comets: Results from Narrowband Photometry of 85 Comets", *Icarus* **118**, 223.

A'Hearn, M. F.; D. G. Schleicher; P. D. Feldman; R. L. Millis; and D. T. Thompson (1984). "Comet Bowell 1980b", *Astron. J.* **89**, 579.

Bianchi, S.; A. Ferrara; and C. Giovanardi (1996). "Monte Carlo Simulations of Dusty Spiral Galaxies: Extinction and Polarization Properties", *Astrophys. J.* **465**, 127.

Błecka, M. I.; and A. Jurewicz (1998). "Seasonal Variations of the Solar Radiation Scattered from the Putative Dust Rings of Mars: A Possible Basis for Photometric Searches", *Astron. Astrophys.* **337**, 955.

Bobrovnikoff, N. T. (1931). "Halley's Comet in its Apparition of 1909-1911", *Publ. Lick Obs.* **17**, 309-482.

Bohren, C. F.; and D. R. Huffman (1983). *Absorption and Scattering of Light by Small Particles* (New York: John Wiley & Sons).

Bortle, J. E. (1976). In "Comet West in the Morning Sky", *Sky Tel.* **51**(4), 219 and 240-241.

Bortle, J. E. (1997a). "Great Comets in History", *Sky Tel.* **93**(1), 44.

Bortle, J. E. (1997b). "How Important is Forward-Scatter Geometry?", *Sky Tel.* **94**(3), 12.

Brownlee, D. E. (1978). "Microparticle Studies by Sampling Techniques", in *Cosmic Dust*, ed. by J. A. M. McDonnell (New York: Wiley), 295-335.

Buratti, B. J.; M. D. Hicks; L. A. Soderblom; D. Britt; J. Oberst; and J. K. Hillier (2004). "Deep Space 1 Photometry of the Nucleus of Comet 19P/Borrelly", *Icarus* **167**, 16.

Burns, J. A.; D. P. Simonelli; M. R. Showalter; D. P. Hamilton; C. C. Porco; L. W. Esposito; and H. Throop (2004). "Jupiter's Ring-Moon System", in *Jupiter: The Planet, Satellites and Magnetosphere*, ed. by F. Bagenal, T. E. Downing, and W. B. McKinnon (Cambridge University Press), 241.

Chaubey, U. S. (1978). "Spectrophotometry of Comet West (1975n) After the Perihelion Passage", *Astrophys. Space Sci.* **54**, 233.

Cox, A. N. (2000). *Allen's Astrophysical Quantities*, 4th edition (New York: Springer-Verlag).

De Almeida, A. A.; P. D. Singh; and W. F. Huebner (1997). "Water Release Rates, Active Areas, and Minimum Nuclear Radius Derived from Visual Magnitudes of Comets — An Application to Comet 46P/Wirtanen", *Planet. Space Sci.* **45**, 681.

Draine, B. T. (2003). "Scattering by Interstellar Dust Grains. I. Optical and Ultraviolet", *Astrophys. J.* **598**, 1017.

Festou, M. C.; H. U. Keller; and H. A. Weaver (2004a). "A Brief Conceptual History of Cometary Science", in Festou *et al.* (2004b), p. 3.

Festou, M. C.; H. U. Keller; and H. A. Weaver (2004b), eds. *Comets II* (Tucson: University of Arizona Press).

Finson, M. L., and R. F. Probstein (1968). "A Theory of Dust Comets. I. Model and Equations", *Astrophys. J.* **154**, 327.

Fulle, M. (2004). "Motion of Cometary Dust", in Festou *et al.* (2004b), p. 565.

Gehrz, R. D. (1997). "Infrared Observations of Comets", *ICQ* **19**, 55.

Gehrz, R. D.; and E. P. Ney (1992). "0.7 to 23 μm Photometric Observations of P/Halley 1986 III and Six Recent Bright Comets", *Icarus* **100**, 162.

Gehrz, R. D.; E. P. Ney; J. Piscitelli; E. Rosenthal; and A. T. Tokunaga (1989). "Infrared Photometry and Spectroscopy of Comet P/Encke in 1987", *Icarus* **80**, 280.

Gibson, S. J.; and K. H. Nordsieck (2003). "The Pleiades Reflection Nebula. II. Simple Model Constraints on Dust Properties and Scattering Geometry", *Astrophys. J.* **589**, 362.

Giese, R. H. (1963). "Light Scattering by Small Particles and Models of Interplanetary Matter Derived from the Zodiacal Light", *Space Sci. Rev.* **1**, 589.

Giese, R. H. (1980). "Optical Investigation of Dust in the Solar System", in Halliday and McIntosh (1980), p. 1.

Goodhue, J. E. (1928). "Skjellerup's Comet Discovered Anew", *Pop. Astron.* **36**, 135.

Goraya, P. S.; B. K. Sinha; U. S. Chaubey; and B. B. Sanwal (1982). "Spectrophotometry of Comet Bradfield (1980t) During Post-perihelion Period", *Moon and Planets* **26**, 3.

Green, D. W. E.; and C. S. Morris (1987). "The Visual Brightness Behavior of P/Halley during 1981-1987", *Astron. Astrophys.* **187**, 560.

Green, D. W. E.; H. Rickman; A. C. Porter; and K. J. Meech (1990). "The Strange Periodic Comet Machholz", *Science* **247**, 1063.

Greenberg, J. M. (1980). "From Interstellar Dust to Comets to the Zodiacal Light", in Halliday and McIntosh (1980), p. 343.

Greenberg, J. M. (1982). "What are Comets Made of? A Model Based on Interstellar Dust", in Wilkening (1982), p. 131.

Greenberg, J. M. (1986). "Predicting that Comet Halley is Dark", *Nature* **321**, 385.

Greenberg, J. M. (1998). "Making a Comet Nucleus", *Astron. Astrophys.* **330**, 375.

Greenberg, J. M. (2000). "The Secrets of Stardust", *Scientific American* **283**(6), 46.

Greenberg, J. M.; and B. Å. S. Gustafson (1981). "A Comet Fragment Model for Zodiacal Light Particles", *Astron. Astrophys.* **93**, 35.

Greenberg, J. M.; and J. I. Hage (1990). "From Interstellar Dust to Comets: A Unification of Observational Constraints", *Astrophys. J.* **361**, 260.

Greenberg, J. M.; and A. Li (1997). "Silicate Core-Organic Refractory Mantle Particles as Interstellar Dust and as Aggregated in Comets and Stellar Disks", *Adv. Space Res.* **19**, 981.

Greenberg, J. M.; N. E. Pedersen; and J. C. Pedersen (1961). "Microwave Analog to the Scattering of Light by Non-spherical Particles", *J. Appl. Phys.* **32**, 233.

Grynko, Y. (2005). "Light Scattering by Cometary Dust Particles with Sizes Large Compared to the Wavelength of Light", Ph.D. dissertation, University of Göttingen (World Wide Web URL `http://meetings.mps.mpg.de/homes/grynko/thesis/thesis.pdf`), 2005 April.

Grynko, Y.; K. Jockers; and R. Schwenn (2004). "The Phase Curve of Cometary Dust: Observations of Comet 96P/Machholz 1 at Large Phase Angle with the SOHO LASCO C3 Coronograph", *Astron. Astrophys.* **427**, 755.

Gustafson, B. Å. S. (1996). "Optical Properties of Dust from Laboratory Scattering Measurements", in *Physics, Chemistry, and Dynamics of Interplanetary Dust*, ed. by B. Å. S. Gustafson and M. S. Hanner; ASP Conference Series, **104**, 401.

Gustafson, B. Å. S.; and Kolokolova, L. (1999). "A Systematic Study of Light Scattering by Aggregate Particles using the Microwave Analog Technique: Angular and Wavelength Dependence of Intensity and Polarization", *J. Geophys. Res.* **104**, 31711.

Hadamcik, E.; J. B. Renard; J. C. Worms; A. C. Levasseur-Regourd; and M. Masson (2002). "Polarization of Light Scattered by Fluffy Particles (PROGRA2 Experiment)", *Icarus* **155**, 497.

Halliday, I.; and B. A. McIntosh (1980), eds. *Solid Particles in the Solar System* (Dordrecht, The Netherlands: D. Reidel Publishing Co.).

Haltrin, V. I. (2002). "One-parameter Two-term Henyey-Greenstein Phase Function for Light Scattering in Seawater", *Appl. Optics* **41**, 1022.

Hanner, M. S.; R. H. Giese; K. Weiss; and R. Zerull (1981). "On the Definition of Albedo and Application to Irregular Particles", *Astron. Astrophys.* **104**, 42.

Hanner, M. S.; and R. L. Newburn (1989). "Infrared Photometry of Comet Wilson (1986l) at Two Epochs", *Astron. J.* **92**, 254.

Hanner, M. S.; E. Tedesco; A. T. Tokunaga; G. J. Veeder; D. F. Lester; F. C. Witteborn; J. D. Bregman; J. Gradie; and L. Lebofsky (1985). "The Dust Coma of Periodic Comet Churyumov-Gerasimenko (1982 VIII)", *Icarus* **64**, 11.

Hartmann, J. (1927). "Komet Skjellerup-Maristany", *Astron. Nachr.* **231**, 413.

Henyey, L. G.; and J. L. Greenstein (1941). "Diffuse Radiation in the Galaxy", *Astrophys. J.* **93**, 70.

Hoag, A. A. (1984). "First Infrared Observations of a Comet", *Bull. Amer. Astron. Soc.* **16**, 942.

Hong, S. S. (1985). "Henyey-Greenstein Representation of the Mean Volume Scattering Phase Function for Zodiacal Dust", *Astron. Astrophys.* **146**, 67.

Howell, E. S.; B. L. Lutz; and V. M. Slipher (1991). "Gas and Dust Production by Comet P/Halley (1910 II)", *Astrophys. J.* **371**, 776.

Jewitt, D. (1991). "Cometary Photometry", in *Comets in the Post-Halley Era* (Dordrecht, Netherlands: Kluwer Academic Publishers), p. 19.

Jockers, K. (1997). "Observations of Scattered Light from Cometary Dust and Their Interpretation", *Earth, Moon, and Planets* **79**, 221.

Jockers, K.; N. Kiselev; T. Bonev; V. Rosenbush; N. Shakhovskoy; S. Kolesnikov; Y. Efimov; D. Shakhovskoy; and K. Antonyuk (2005). "CCD Imaging and Aperture Polarimetry of Comet 2P/Encke: Are There Two Polarimetric Classes of Comets?", *Astron. Astrophys.* **441**, 773.

Kalas, P.; and D. Jewitt (1995). "Asymmetries in the β Pictoris Dust Disk", *Astron. J.* **110**, 794.

Kempf, S.; U. Beckmann; M. Burton; S. Helfert; R. Srama; G. Moragas-Klostermeyer; M. Roy; and E. Gruen (2005). "Saturn's E Ring as Seen by Cassini", American Geophysical Union, Fall Meeting 2005, abstract #P31D-05.

Kimura, H.; L. Kolokolova; and I. Mann (2003). "Optical Properties of Comet Dust: Constraints from Numerical Studies on Light Scattering by Aggregate Particles", *Astron. Astrophys.* **407**, L5.

Kimura, H.; L. Kolokolova; and I. Mann (2006). "Light Scattering by Cometary Dust Numerically Simulated with Aggregate Particles Consisting of Identical Spheres", *Astron. Astrophys.* **449**, 1243.

Kimura, H.; I. Mann; D. A. Biesecker; and E. K. Jessberger (2002). "Dust Grains in the Comae and Tails of Sungrazing Comets: Modeling of Their Mineralogical and Morphological Properties", *Icarus* **159**, 529.

Kiselev, N. N.; and G. P. Chernova (1981). "Phase Functions of Polarization and Brightness and the Nature of Cometary Atmosphere Particles", *Icarus* **48**, 473.

Kolokolova, L.; M. S. Hanner; A.-N. Levasseur-Regourd; and B. Å. S. Gustafson (2004a). "Physical Properties of Cometary Dust from Light Scattering and Thermal Emission", in Festou *et al.* (2004b), p. 577.

Kolokolova, L.; and H. Kimura (2006). "A Model of Comet Dust Based on Integrated Remote-sensing Data", Asia Oceanic Geosciences Society 3rd Annual Meeting, Suntec, Singapore, 2006 July 10-14, Abstract 59-PS-A0300.

Kolokolova, L.; H. Kimura; and I. Mann (2004b). "Characterization of Dust Particles using Photopolarimetric Data: Example of Cometary Dust", in *Photopolarimetry in Remote Sensing*, ed. by G. Videen, Y. Yatskiv and M. Mischenko (Dordrecht, The Netherlands: Kluwer Academic Publishers), p. 431.

Kozasa, T.; J. Blum; H. Okamoto; and T. Mukai (1993). "Optical Properties of Dust Aggregates. II. Angular Dependence of Scattered Light", *Astron. Astrophys.* **276**, 278.

Krasnopolsky, V. A.; V. I. Moroz; A. A. Krysko; A. Y. Tkachuk; G. Moreels; J. Clairmidi; J. P. Parison; M. Gogoshev; and T. Gogosheva (1987). "Properties of Dust in Comet P/Halley Measured by the Vega-2 Three-channel Spectrometer", *Astron. Astrophys.* **187**, 707.

Lamers, H. J. G. L. M.; A. Lecavelier des Etangs; and A. Vidal-Madjar (1997). "β Pictoris Light Variations. II. Scattering by a Dust Cloud", *Astron. Astrophys.* **328**, 321.

Lampland, C. O. (1928). "Radiometric Observations of Skjellerup's Comet", *Pop. Astron.* **36**, 240.

Lara, L.-M.; G. P. Tozzi; H. Boehnhardt; M. DiMartino; and R. Schulz (2004). "Gas and Dust in Comet C/2000 WM1 During its Closest Approach to Earth: Optical Imaging and Long-slit Spectroscopy", *Astron. Astrophys.* **422**, 717.

Lemmon, M. T.; M. J. Wolff; M. D. Smith; R. T. Clancy; D. Banfield; G. A. Landis; A. Ghosh; P. H. Smith; N. Spanovich; B. Whitney; P. Whelley; R. Greeley; S. Thompson; J. F. Bell III; and S. W. Squyres (2004). "Atmospheric Imaging Results from the Mars Exploration Rovers: Spirit and Opportunity", *Science* **306**, 1753.

Levasseur-Regourd; A. C., E. Hadamcik; and J. B. Renard (1996). "Evidence of Two Classes of Comets from Their Polarimetric Properties at Large Phase Angles", *Astron. Astrophys.* **313**, 327.

Li, A.; and J. M. Greenberg (1998). "From Interstellar Dust to Comets: Infrared Emission from Comet Hale-Bopp (C/1995 O1)", *Astrophys. J.* **498**, L83.

Lisse, C. M.; Y. R. Fernández; M. F. A'Hearn; E. Grün; H. U. Käaff; D. J. Osip; D. J. Lien; T. Kostiuk; S. B. Peschke; and R. G. Walker (2004). "A Tale of Two Very Different Comets: ISO and MSX Measurements of Dust Emission from 126P/IRAS (1996) and 2P/Encke (1997)", *Icarus* **171**, 444.

Mann, I.; H. Kimura; and L. Kolokolova (2004). "A Comprehensive Model to Describe Light Scattering Properties of Cometary Dust", *J. Quant. Spectrosc. Radiat. Transfer* **89**, 291.

Marcus, J. N. (1986). "Halley in the Daytime", Sky Telesc. **71**(2), 125.

Marcus, J. N. (1997). "Great Comet Geometry", Sky Telesc. **93**(4), 8.

Marcus, J. N. (2001). "J. Mayo Greenberg (1922-2001)", *ICQ* **23**, 153.

Marcus, J. N. (2004). "Forward-scatter Enhancement of Comet Brightness", presentation at the Third International Workshop on Cometary Astronomy (IWCA III), Meudon, France, 2004 June 4-6.

Marcus, J. N. (2007a). "The First Infrared Observations of a Comet: Carl Lampland's Radiometry of C/1927 X1", in preparation.

Marcus, J. N. (2007b). "C/2006 P1 (McNaught)", *IAU Circular* 8793, 2007 Jan. 11.

Marcus, J. N. (2007c). "Updated Brightness Forecast for Comet C/2006 P1 (McNaught) in Daylight with Predicted Forward-scattering Brightness Boost", World Wide Web URL `http://shopplaza.nl/astro`, Jan. 2.

Marcus, J. N.; and D. A. J. Seargent (1986). "Dust Forward Scatter Brightness Enhancement in Previous Apparitions of Halley's Comet", in *Proc. 20th ESLAB Symposium on the Exploration of Halley's Comet*, ESA SP-250, ed. by B. Battrick, E. J. Rolfe, and R. Reinhard (Noordwijk: ESA/ESTEC), Vol. 3, 359-362.

Mason, C. G.; R. D. Gehrz; E. P. Ney; and D. M. Williams (1998). "The Temporal Development of the Pre-perihelion Infrared Spectral Energy Distribution of Comet Hyakutake (C/1996 B2)", *Astrophys. J.* **507**, 398.

Mason, C. G.; R. D. Gehrz; T. J. Jones; C. E. Woodward; M. S. Hanner; and D. M. Williams (2001). "Observations of Unusually Small Dust Grains in the Coma of Comet Hale-Bopp (C/1995 O1)", *Astrophys. J.* **549**, 635.

McDonnell, J. A. M.; W. M. Alexander; W. M. Burton; E. Bussoletti; G. C. Evans; S. T. Evans; J. G. Firth; and 21 additional authors (1987). "The Dust Distribution Within the Inner Coma of Comet P/Halley 1982i: Encounter by Giotto's Impact Detectors", *Astron. Astrophys.* **187**, 719.

Meech, K. J.; and D. C. Jewitt (1987). "Observations of Comet P/Halley at Minimum Phase Angle", *Astron. Astrophys.* **187**, 585.

Meisel, D. D.; and C. S. Morris (1982). "Comet Head Photometry: Past, Present, and Future", in Wilkening (1982), p. 341.

Middleton, W. E. K. (1951). "Visibility in Meteorology", in *Compendium of Meteorology*, ed. by T. F. Malone (Boston: American Meteorological Society), p. 91.

Milani, G. (2005). "The CARA Project and the $Af\rho$ Approach to Cometary Photometry", *ICQ* **27**, 240.

Millis, R. L.; M. F. A'Hearn; and D. T. Thompson (1982). "Narrowband Photometry of Comet P/Stephan-Oterma and the Backscattering Properties of Cometary Grains", *Astron. J.* **87**, 1310.

Mie, G. (1908). "Beiträge zur Optik Trüber Medien, Speziel Kolloidaler Metallösungen", *Ann. Physik* **25**, 377.

Morris, C. S. (1973). "On Aperture Corrections for Comet Magnitude Estimates", *Publ. Astron. Soc. Pacif.* **85**, 470.

Muñoz, O.; F. Moreno; A. Molina; and J. L. Ortiz (1999). "A Comparison of the Structure of the Aerosol Layers in the Great Red Spot of Jupiter and its Surroundings Before and After the 1993 SEB Disturbance", *Astron. Astrophys.* **344**, 355.

Newburn, R. L., Jr. (1981). "A Semi-empirical Photometric Theory of Cometary Gas and Dust Production: Application to P/Halley's Gas Production Rates", in *The Comet Halley Gas and Dust Environment* (Paris: European Space Agency), ESA SP-174, p. 3.

Newburn, R. L., Jr. (1984). "A New Calibration of the Semi-empirical Photometric Theory for Halley and Other Comets", *Adv. Space Res.* **4**, 185.

Ney, E. P. (1982). "Optical and Infrared Observations of Bright Comets in the Range 0.5 μm to 20 μm", in Wilkening (1982), p. 323.

Ney, E. P.; and K. M. Merrill (1976). "Comet West and the Scattering Function of Cometary Dust", *Science* **194**, 1051.

Pang, K. D.; C. C. Voge; and J. M. Ajello (1984). "The E ring of Saturn and Satellite Enceladus", *J. Geophys. Res.* **89**, 9459.

Patat, F. (2005). "Reflections on Reflexions: I. Light Echoes in Type Ia Supernovae", *Mon. Not. R. Astron. Soc.* **357**, 1161.

Petrova, E. V.; K. Jockers; and N. N. Kiselev (2000). "Light Scattering by Aggregates with Sizes Comparable to the Wavelength: An Application to Cometary Dust", *Icarus* **148**, 526.

Porco, C. C.; R. A. West; A. McEwen; A. D. Del Genio; A. P. Ingersoll; P. Thomas; S. Squyres; and 17 additional authors (2003). "Cassini Imaging of Jupiter's Atmosphere, Satellites, and Rings", *Science* **299**, 1541.

Richter, N. B. (1963). *The Nature of Comets*, translated by A. Beer (London: Methuen).

Schleicher, D. G.; R. L. Millis; and P. V. Birch (1998). "Narrowband Photometry of Comet P/Halley: Variation with Heliocentric Distance, Season, and Solar Phase Angle", *Icarus* **132**, 397.

Schmidt, J. F. J. (1863). "Astronomische Beobachtungen über Cometen", *Publ. Obs. Athens* (Athens: Wilberg), Series 1, Vol. 4.
Sekanina, Z. (1982). "The Path and Surviving Tail of a Comet that Fell into the Sun", *Astron. J.* **87**, 1059.
Sekanina, Z. (1990). "Periodic Comet Machholz and its Idiosyncrasies", *Astron. J.* **99**, 1268.
Sekanina, Z.; and P. W. Chodas (2005). "Origin of the Marsden and Kracht Groups of Sunskirting Comets. I. Association with Comet 96P/Machholz and its Interplanetary Complex", *Astrophys. J. Suppl. Ser.* **161**, 551.
Sekanina, Z.; M. S. Hanner; E. K. Jessberger; and M. N. Fomenkova (2001). "Cometary Dust", in *Interplanetary Dust*, ed. by E. Grün, B. Å. S. Gustafson, S. F. Dermott, and H. Fechtig (Berlin and Heidelberg: Springer-Verlag), p. 95.
Soderblom, L. A.; T. I. Becker; G. Bennett; D. C. Boice; D. T. Britt; R. H. Brown; B. J. Buratti; and 15 additional authors (2002). "Observations of Comet 19P/Borrelly by the Miniature Integrated Camera and Spectrometer aboard Deep Space 1", *Science* **296**, 1087.
Storrs, A. D.; A. L. Cochran; and E. S. Barker (1992). "Spectrophotometry of the Continuum in 18 Comets", *Icarus* **98**, 163.
Tenn, J. S. (2007). "Lowell Observatory Enters the Twentieth Centurey — in the 1950s", *J. Astron. Hist. and Heritage* **10**(1), 65.
Thorpe, T. E. (1981). "Mars Atmospheric Opacity Effects Observed in the Northern Hemisphere by Viking Orbiter imaging", *J. Geophys. Res.* **86**, 11419.
Tomasko, M. G.; R. S. McMillan; L. R. Doose; N. D. Castillo; and J. P. Dilley (1980). "Photometry of Saturn at Large Phase Angles", *J. Geophys. Res.* **85**, 5891.
Vaidya, D. B.; and J. N. Desai (1986). "Detection of Submillimeter Size Particles in the Inner Coma of a Comet Through Their Forward Scattering", *Earth, Moon, and Planets* **35**, 7.
Van Biesbroeck, G. (1928). "Comet Notes", *Pop. Astron.* **36**, 117.
Van de Hulst, H. C. (1980). *Multiple Light Scattering: Tables, Formulas, and Applications*, Vol. 2 (New York: Academic Press).
Van de Hulst, H. C. (1981). *Light Scattering by Small Particles* (New York: Dover Publications, Inc.).
Vanýsek, V. (1968). "The Possibility of a Forward Scattering Effect in the Continuous Spectra of Comets", *Icarus* **8**, 1.
Volz, F. E. (1983). "Volcanic Turbidity, Skylight Scattering Functions, and Neutral Points in New England 1982/83", *Proc. 5th Conference on Atmospheric Radiation, 31 Oct.-4 Nov.* (Baltimore: American Meteorological Society), p. 1.
Weaver, H. A. (2004). "Not a Rubble Pile?", *Science* **304**, 1760.
Wells, H. G. (1924). *In the Days of the Comet* (New York: Charles Scribner's Sons), p. 79 (chapter 2, section 7).
Whipple, F. L. (1951). "A Comet Model. II. Physical Relations for Comets and Meteors", *Astrophys. J.* **113**, 464.
Whipple, F. L. (1987). "The Cometary Nucleus: Current Concepts", *Astron. Astrophys.* **187**, 852.
Wilkening, L. L. (1982), ed. *Comets* (Tucson: University of Arizona Press).
Wilson, J. G. (1951). *The Principles of Cloud Chamber Technique* (Cambridge University Press).
Yanamandra-Fisher, P. A. and M. S. Hanner (1999). "Optical Properties of Nonspherical Particles of Size Comparable to the Wavelength of Light: Application to Comet Dust", *Icarus* **138**, 107.
Yeomans, D. K. (1991). *Comets: A Chronological History of Observation, Science, Myth, and Folklore* (New York: John Wiley & Sons, Inc.).
Zerull, R. H.; B. Å. S. Gustafson; K. Schulz; and E. Thiele-Corbach (1993). "Scattering by Aggregates With and Without an Absorbing Mantle: Microwave Analog Experiments", *Appl. Optics* **32**, 4088.

Φ Φ Φ

Observations of Comet C/2006 P1

Due to the high cost of printing this April issue on glossy paper and in color — indeed, we have never before done this — all observations of comets other than C/2006 P1 are being delayed to the July issue. We have never before made one comet the complete focus of published observations in the *ICQ*, but then again, C/2006 P1 was a special comet — the brightest comet to grace our skies since C/1965 S1 (Ikeya-Seki). This means that some observations that had been delayed from the January issue (other than those of C/2006 P1) are being shunted into the July issue. Lest readers be concerned at the delay in publishing the observations of other comets, the July issue was being prepared jointly with the April issue from an editorial standpoint, and it will be printed and mailed within a month of the April issue — sometime in August. — *the Editor*

New CCD-data instrumentation abbreviation codes: *CCD camera:* `SXV` = *Starlight Xpress SXV-H9. CCD camera chip:* `ICY` = *Sony ICX285AL. Computer software used for photometric reduction of CCD images:* `AIP` = *"AIP for Windows" (Berry and Burnell).*

Descriptive Information, to complement the Tabulated Data (all times UT):

See the July 2001 issue (page 98) for explanations of the abbreviations used in the descriptive information.

◇ *Comet C/2006 P1 (McNaught)* ⟹ 2007 Jan. 3.49: w/ 15×80 B, $m_1 \approx 2$, coma dia ≈ 1′, DC = 8; "twilight was very far advanced when I picked up the comet, but it is obviously very bright; in fact, my view harkened back to my final